Check for updates
ADVANCED ELECTRONIC MATERIALS Open Access
www.advelectronicmat.de

Emerging Optoelectronic Devices for Brain-Inspired Computing

Lingxiang Hu, Xia Zhuge, Jingrui Wang, Xianhua Wei, Li Zhang, Yang Chai, Xiaoyong Xue, Zhizhen Ye, and Fei Zhuge**

Brain-inspired neuromorphic computing is recognized as a promising technology for implementing human intelligence in hardware. Neuromorphic devices, including artificial synapses and neurons, are regarded as essential components for the construction of neuromorphic hardware systems. Recently, optoelectronic neuromorphic devices are increasingly highlighted due to their potential applications in next-generation artificial visual systems, attributed to their integrated sensing, computing, and memory capabilities. In this review, recent advancements in optoelectronic synapses and neurons are examined, with an emphasis on their structural characteristics, operational principles, and the replication of neuromorphic functions. For optoelectronic synaptic devices, such as memristor- and transistor-based ones, attention is given to the two primary weight update modes: the light-electricity synergistic mode and the all-optical mode. Optoelectronic neurons are discussed in terms of different device types, including threshold switch neurons and semiconductor laser neurons. Last, the challenges that impede the progress of optoelectronic neuromorphic devices are identified, and potential future directions are suggested.

1. Introduction

The human brain is often described as a biological computer with a remarkably low power consumption of 20 W.[1] However, it surpasses digital computers in performing complex fuzzy computing tasks, such as decision-making. Artificial intelligence (AI) is defined as the ability of machines to imitate human intelligence, with these machines being designed to carry out tasks that demand human intelligence, such as image recognition, natural language understanding, and gaming. Despite the significant impact AI has had on various aspects of society, it still falls short compared to human intelligence. Although tasks can often be completed more efficiently by AI than by humans, AI's capabilities remain confined to specific algorithms, limiting its operations to predetermined functions.

L. Hu, J. Wang, F. Zhuge
Ningbo Institute of Materials Technology and Engineering
Chinese Academy of Sciences
Ningbo 315201, China
E-mail: zhugefei@nimte.ac.cn

X. Zhuge, J. Wang
School of Electronic and Information Engineering
Ningbo University of Technology
Ningbo 315211, China

X. Wei
State Key Laboratory of Environment-friendly Energy Materials
Southwest University of Science and Technology
Mianyang 621010, China

L. Zhang
Healthcare Engineering Centre
School of Engineering
Temasek Polytechnic
Tampines Ave
Singapore 529757, Singapore

The ORCID identification number(s) for the author(s) of this article can be found under https://doi.org/10.1002/aelm.202400482

© 2024 The Author(s). Advanced Electronic Materials published by Wiley-VCH GmbH. This is an open access article under the terms of the Creative Commons Attribution License, which permits use, distribution and reproduction in any medium, provided the original work is properly cited.

DOI: 10.1002/aelm.202400482

Y. Chai
Department of Applied Physics
The Hong Kong Polytechnic University
Hong Kong 999077, China

X. Xue
School of Microelectronics
Fudan University
Shanghai 201203, China
E-mail: xuexiaoyong@fudan.edu.cn

Z. Ye
State Key Laboratory of Silicon and Advanced Semiconductor Materials
School of Materials Science and Engineering
Zhejiang University
Hangzhou 310027, China

Z. Ye, F. Zhuge
Institute of Wenzhou
Zhejiang University
Wenzhou 325006, China

F. Zhuge
Center for Excellence in Brain Science and Intelligence Technology
Chinese Academy of Sciences
Shanghai 200072, China

2199160x, 2025, 3, Downloaded from https://advanced.onlinelibrary.wiley.com/doi/10.1002/aelm.202400482 by HONG KONG POLYTECHNIC UNIVERSITY HU NG HOM, Wiley Online Library on [24/02/2026]. See the Terms and Conditions (https://onlinelibrary.wiley.com/terms-and-conditions) on Wiley Online Library for rules of use; OA articles are governed by the applicable Creative Commons License

Moreover, AI algorithms are typically run on digital computers, which encounter the von Neumann Bottleneck or memory wall issue due to the memory's slower speed compared to the central processing unit (CPU), leading to periods of CPU inactivity.[2] Consequently, current AI technologies are considered lacking in terms of both hardware and software.

Inspired by the neural structure and operating principles of the human brain, neuromorphic computing (NC) is regarded as the next generation of AI.[2,3] Briefly, NC aims to implement AI by constructing an artificial brain mainly composed of artificial neurons and synapses. Similar to the human brain, an ideal neuromorphic system is expected to perform in-memory computing based on the synaptic weight update rule of spike-timing-dependent plasticity (STDP)[4–8] in a massively parallel mode, potentially surpassing digital computers in computing speed and energy efficiency, especially for complex fuzzy tasks. An example of neuromorphic architecture is IBM's TrueNorth chip, which consists of 1 million spiking neurons and 256 million synapses utilizing complementary metal–oxide–semiconductor (CMOS) technology.[9] It can execute AI tasks in real time using intricate neural networks, such as multi-object detection and classification, with minimal power consumption of 63 mW. The TrueNorth chip, mimicking neural or synaptic function through a CMOS circuit primarily made of transistors, incorporates 5.4 billion transistors. In addition to CMOS integrated circuit technology, emerging memory devices such as memristive devices,[10–25] transistors,[26–35] phase change devices,[36–43] magnetoresistive devices,[15,44–50] and ferroelectric devices[51–57] have also been shown to function as artificial neurons and synapses. These devices can exhibit neural or synaptic behavior without complex electronic circuits, allowing neuromorphic chips made from them to achieve an extremely high integration density, potentially comparable to that of the human brain.

A significant amount of research has been conducted on the development of electronic neuron and synapse devices, which respond to electrical signals.[58–62] Neuromorphic chips created using these electronic devices face a challenge due to the mismatch in the enhancement rate between off-chip I/O bandwidth and internal chip performance.[63] Light has long been recognized as a promising medium for matrix multiplication and interconnects.[64] Optoelectronic devices activated by optical signals offer higher bandwidth, reduced cross talk, and lower power consumption compared to electronic devices.[65–71] For instance, an artificial optic-neural synapse consumes only 66 fJ per spike;[72] and a neuromorphic visual system utilizing photodiode arrays can classify and encode optically projected images at a speed of 20 million bins per second.[73]

The human brain comprises ≈10^{11} neurons and around 10^{15} synapses.[74] Each neuron is connected to other neurons through 10^3–10^4 synapses. Neurons initiate action potentials once their membrane potentials reach specific threshold levels[75,76] and transmit them to the next neuron via chemical or electrical synapses. Optoelectronic neurons are capable of performing the dual functions of a photodetector and leaky integrator.[22,77,78] They generate electrical or optical spikes when the integrated pulse-position-modulation optical signals surpass certain thresholds and relay these information spikes to other neurons through synaptic connections. As early as 1989,[79] a fundamental optoelectronic circuit mimicking an artificial neuron was developed, and a basic content addressable memory was established using optical interconnections based on the Hopfield model. Subsequently, numerous research breakthroughs in optoelectronic neuron circuits have since been documented.[80–84] Notably, a photoresponsive single-transistor neuron has been introduced, enabling optical sensing and neuromorphic capabilities within a single device.[85]

Synapses are recognized as the fundamental elements of learning and memory in the brain.[86] Signal transmission between neurons, as well as to non-neural cells such as muscle fibers, is enabled by synapses.[87] A key feature of synapses is their ability to track the history of neural activity, which is stored in various patterns of activity-dependent plasticity, forming the foundation of learning and memory. Optoelectronic synapses have been demonstrated to adjust device conductance reversibly using solely optical signals[88,89] or a combination of electrical and optical signals.[90–94] The first optoelectronic synapse was achieved in 2010 with an optically gated carbon nanotube transistor.[95] Subsequently, different optoelectronic devices have been discovered to display light-tunable synaptic behaviors.[90–94,96–101] In 2020,[88,89] the all-optically controlled (AOC) synaptic device with long-term plasticity was unveiled, utilizing a bilayer InGaZnO (IGZO) memristor.

Optoelectronic neuromorphic devices are positioned as strong contenders for future neuromorphic visual systems due to their potential for integrated sensing-computing-memory (ISCM). This review outlines the latest progress in the advancement of optoelectronic synapses and neurons, with an emphasis on their structures and operational principles.

2. Optoelectronic Synapses

A synapse is typically defined as a connection between the axon of one neuron and the soma of another.[86] The fundamental requirement for a synaptic device is that its conductance, serving as synaptic weight, can be reversibly tuned. In most synaptic devices, weights updates are driven by electrical stimuli. In contrast, optoelectronic synapses involve weight updates using optical stimuli, allowing the advantages of both photonics and electronics to be combined. Various types of optoelectronic synapses are explored here based on their device structures and weight update methods.

2.1. Optoelectronic Memristors

The memristor,[102] with memristance M, is considered the fourth fundamental two-terminal circuit element alongside the resistor, inductor, and capacitor. It describes the differential relationship between charge (q) and flux (φ) as $d\varphi = M dq$. The existence of the memristor was predicted by Leon Chua[102] in 1971 based on symmetry arguments. In 2008, Hewlett-Packard Labs[103] identified resistive switching devices as a type of memristor through combined theoretical and experimental analysis. Due to their charge-controlled nonlinear resistance (or conductance) switching behaviors, memristors are seen as promising candidates for artificial synapses.[2–4,10–14,16,90,104–107] Compared to electronic memristors, research on optoelectronic memristors

© 2024 The Author(s). Advanced Electronic Materials published by Wiley-VCH GmbH

remains in its early stages. Optoelectronic memristors can be classified into two categories based on the control (i.e., weight update) method: light-electricity synergistic control and all-optical control.

2.1.1. Light-Electricity Synergistic Control

Optical Potentiation and Electrical Depression: In optoelectronic memristors, device conductance can be modified based on the persistent photoconductivity (PPC) effect.[89,90,101,108] Specifically, the conductance of the device increases when exposed to light, and even after the light is removed, the conductance level remains elevated for a prolonged period, usually due to material defects such as oxygen vacancies (V_Os) in oxides.[89,109]

For example, a highly transparent optoelectronic synapse is demonstrated using an all-oxide memristor.[101] The device consists of In_2O_3/ZnO thin films on a fluorine-doped tin oxide (FTO)/glass substrate, depicted in **Figure 1a**. The photocurrent response of the device, following illumination with a single ultraviolet (UV) pulse and subsequent application of electric pulses for a 30 s measurement period, is shown in Figure 1b. It is evident that the current gradually increases with UV illumination due to photogenerated electrons and holes. After UV cessation, a gradual decay in the current is observed, caused by the recombination of photogenerated electrons and holes. Nevertheless, the current does not return to its initial state because photogenerated electrons and holes become trapped by V_Os defects at the In_2O_3/ZnO interface, indicating a PPC behavior. By applying a series of negative voltage pulses, the current level can be reset to its initial value. Figure 1c illustrates the reversible regulation of the synaptic weight, based on the optical potentiation and electrical depression behavior of the In_2O_3/ZnO device. The conductance of the device gradually increases when exposed to consecutive UV pulses, resembling long-term potentiation (LTP). The conductance decreases upon the application of negative voltage pulses, resembling long-term depression (LTD).

The PPC phenomenon is commonly observed in semiconductor materials, especially in oxides. As a result, oxide-based optoelectronic memristors have been extensively studied, including those made from ZnO_{1-x}/AlO_y,[90] ZnO,[110–113] CeO_x/ZnO,[114] ZnO/HfO_x,[115] MoO_x,[116] CeO_{2-x}/AlO_y,[117] TiO_x,[108] Nb:$SrTiO_3$,[118] NiO/ZnO,[119] $BiFeO_3$-$BaTiO_3$,[120] ZnO:N/IGZO,[121] SiO_2,[122] and HfO_x.[123] In addition to oxides, new materials such as low-dimensional materials[91,124–127] and perovskites[128–131] are also commonly utilized in the fabrication of optoelectronic memristive devices.

Electrical Potentiation and Optical Depression: Filamentary memristors, a common type of electrically driven memristor, primarily involve the formation and rupture of a conducting filament (CF) made up of V_Os or metal atoms from the active electrode (e.g., Cu or Ag).[3,10,16,132] The CF links the top and bottom electrodes, switching the device from a high resistance state (HRS) to a low resistance state (LRS). The CF is usually in a metastable state and can fracture due to Joule heat-driven diffusion and high interfacial energy, causing the device to revert from LRS to HRS.[133–135] This presents a potential method for decreasing the conductance of a memristive device through exposure to light.

Tseng and co-workers demonstrated a CF-type memristive device with a structure of ITO/TaO_x/Zn_2SnO_4(ZTO)/ITO.[99] The device exhibits stable bipolar switching behavior. By applying a positive bias to the ITO top electrode (TE), V_Os moves toward the ITO bottom electrode (BE), creating a conical-shaped CF in the oxide layer, as shown in Figure 1d. When a negative bias is imposed on the ITO TE, the CF breaks at the TaO_x/ZTO interface. It is noteworthy that exposure to light can also elevate the device's resistance, similar to the effect of a negative bias (Figure 1e). Initially, without light, the device is switched to LRS by applying a positive bias on the ITO TE (electrical SET). Subsequently, upon exposure to blue light (405 nm) with different power densities, the device's current decreases rapidly, leading to a transition from LRS back to HRS (optical RESET). This finding confirms that light exposure provides adequate energy for oxygen ions to combine with V_Os, destabilizing the CF in the oxide layer. The device's endurance stability is also confirmed through electrical SET and optical RESET operations (Figure 1f).

Memristive synapses based on $CH_3NH_3PbI_3$,[94] $MoSe_2/Bi_2Se_3$,[136] HfO_2,[137] $BiFeO_3/SrRuO_3$,[138] and organic materials[139] demonstrate similar electrical potentiation and optical depression characteristics.

Light-Assisted Electrical Control: Light illumination can enhance the memristive characteristics, such as decreasing the operating voltage[140–145] and increasing the on/off ratio.[100,145–148] For instance, a CF-type memristive device with a structure of Ag/$CH_3NH_3PbI_3$/ITO was fabricated to mimic synaptic functions driven by electrical signals.[145] It is crucial to highlight that light illumination can lower the initiation threshold of LTP and enable the synaptic weights to be updated with smaller electrical pulses. The resistive switching mechanism of the device relies on the formation and rupture of CFs composed of iodine vacancies in $MAPbI_3$. When light is applied to the device, the photogenerated electric field aligns with the positive-bias-produced electric field, boosting the overall electric field and enhancing the migration force of iodine vacancies toward the ITO electrode. Consequently, under light exposure, LTP can be achieved with a reduced electrical input signal.

Further, Peng and co-workers developed a vertical memristive synapse based on Au/KI–$MAPbI_3$/ITO,[100] as depicted in Figure 1g. Various synaptic functions are mimicked using electric stimuli, such as short-term plasticity (STP), LTP, LTD, and spike-number-dependent plasticity. The device can also function as an optoelectronic synapse. Figure 1h illustrates the simulation of LTP and LTD processes of biological synapses by applying a series of positive and negative voltage pulses to the device with and without light illumination. It is evident that a sequence of positive pulses increases the conductance, while negative pulses decrease it. In darkness, the on/off ratio is ≈16. By increasing the light intensity to 0.63 mW cm^{-2}, the on/off ratio increases to 27. This indicates that light illumination expands the conductance regulation range under purely electric stimulation in darkness, thereby improving the device's capability as an artificial synapse. It is worth mentioning that the on/off ratio can also be boosted by applying stronger voltage pulses without light. However, this comes with the trade-off of increased power consumption.

Electricity-Assisted Optical Control: The optoelectronic properties of a memristor are usually influenced by the electrical signal

© 2024 The Author(s). Advanced Electronic Materials published by Wiley-VCH GmbH

2199160x, 2025, 3, Downloaded from https://advanced.onlinelibrary.wiley.com/doi/10.1002/aelm.202400482 by HONG KONG POLYTECHNIC UNIVERSITY HU NG HOM, Wiley Online Library on [24/02/2026]. See the Terms and Conditions (https://onlinelibrary.wiley.com/terms-and-conditions) on Wiley Online Library for rules of use; OA articles are governed by the applicable Creative Commons License

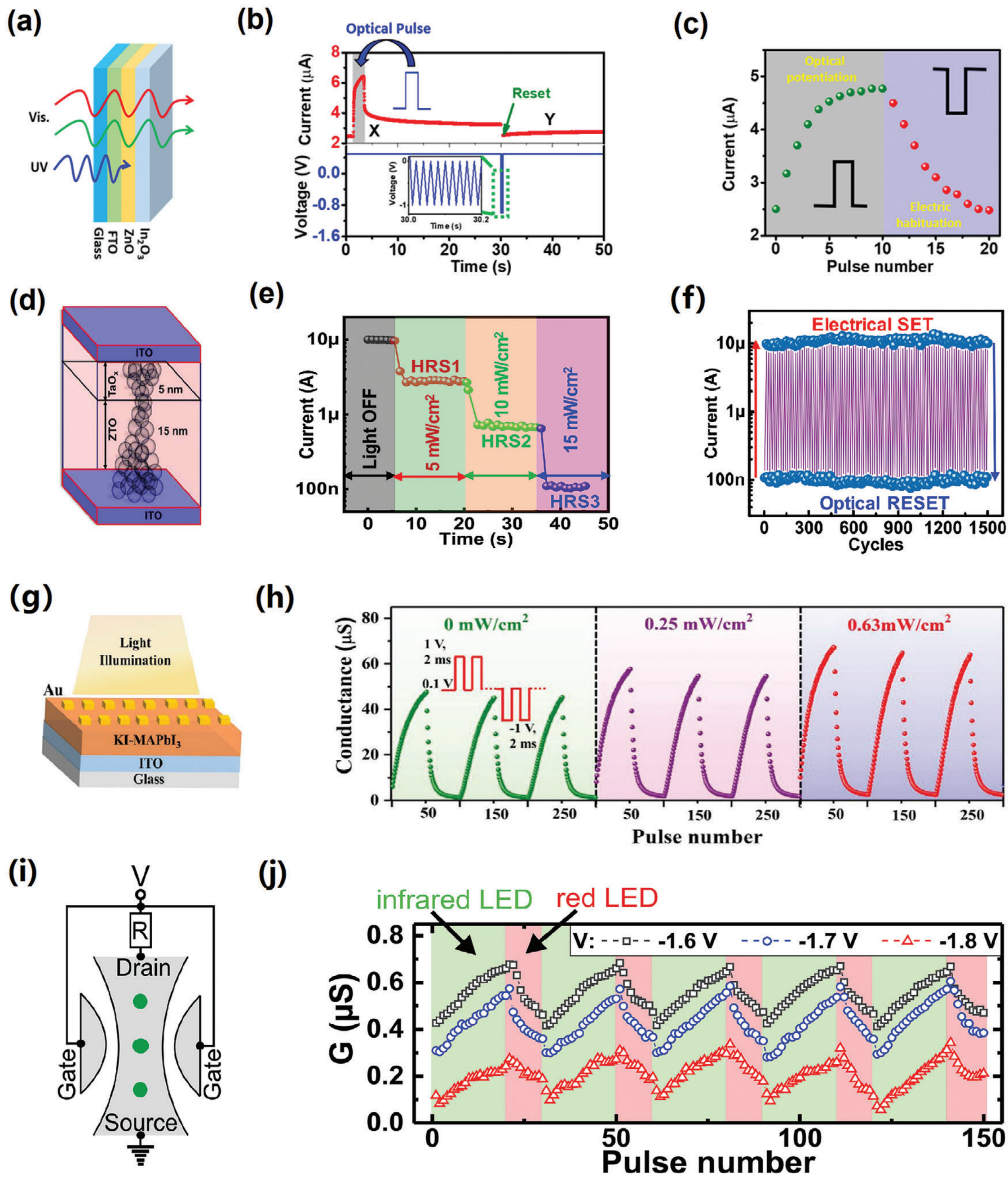

Figure 1. Light-electricity synergistically controlled memristors. a) Schematic illustration of the In_2O_3/ZnO/FTO device. b) Optical potentiation and electrical depression. c) Reversible conductance regulation based on the optical potentiation and electrical depression. Reproduced with permission.[101] Copyright 2018, American Chemical Society (a–c). d) Schematic diagram of the bilayer ITO/TaO_x/ZTO/ITO device. e) Optical RESET processes with different power densities (from 5 to 15 mW cm^{-2}). f) Electrical SET and optical RESET cycles. Reproduced with permission.[99] Copyright 2022, American Chemical Society (d–f). g) Schematic illustration of the KI-$MAPbI_3$-based memristor. h) Reversible conductance regulation using electrical stimulation with and without light illumination. Reproduced with permission.[100] Copyright 2021, Wiley-VCH (g,h). i) Schematic illustration of the four-terminal memristor based on GaAs/AlGaAs and InAs QDs. j) Reversible conductance regulation under infrared and red light illumination at three different bias voltages. Reproduced with permission.[149] Copyright 2016, AIP Publishing (i,j).

applied to the device. Thus, the optoelectronic response of the device can be modified by adjusting the amplitude or polarity of the voltage.[98,149–151]

Hartmann et al. introduced a unique memristor with a four-terminal structure based on GaAs/AlGaAs heterostructure containing InAs quantum dots (QDs),[149] as shown in Figure 1i. By applying two gate biases, the conductance of the device can be increased with infrared light and decreased with red light. As illustrated in Figure 1j, applying bias voltages of −1.6, −1.7, and −1.8 V individually to the device, infrared (red) light causes

 © 2024 The Author(s). Advanced Electronic Materials published by Wiley-VCH GmbH

2199160x, 2025, 3, Downloaded from https://advanced.onlinelibrary.wiley.com/doi/10.1002/aelm.202400482 by HONG KONG POLYTECHNIC UNIVERSITY HU NG HOM, Wiley Online Library on [24/02/2026]. See the Terms and Conditions (https://onlinelibrary.wiley.com/terms-and-conditions) on Wiley Online Library for rules of use; OA articles are governed by the applicable Creative Commons License

a successive increase (decrease) in conductance. As the applied bias voltage decreases, lower peak and valley values of conductance are observed. When the device is illuminated with red light, electron-hole-pairs are generated in the GaAs/AlGaAs heterostructure through interband absorption, leading to a decrease in conductance when more electrons than holes are trapped by InAs QDs. Conversely, exposure to infrared light triggers intraband absorption, causing InAs QD discharge and a subsequent increase in device conductance.

Further, through the use of electricity-assisted mode, both positive and negative PPC effect,[152] as well as the switching of STP to LTP of synapses can be achieved by the optoelectronic memristor.[98]

2.1.2. All-Optical Control

The conductance of AOC memristors can be reversibly modulated under light stimuli. This modulation enables the avoidance of microstructural changes triggered by the electric field and the Joule heat induced by current in electrical memristors. AOC memristor-based neuromorphic devices are considered promising for next-generation vision sensors with integrated sensing, computing, and memory capabilities. Nevertheless, the achievement of AOC memristors remains challenging due to the intrinsic photoelectric effect of semiconductors.[70,71,89,153–156]

The first AOC memristor was developed using an oxygen-deficient InGaZnO (O_D-IGZO)/oxygen-rich IGZO (O_R-IGZO) homojunction[88,89] (**Figure 2a**). The conductance of this device was reversibly tuned by light of different wavelength. For example, blue light at 420 nm and near-infrared (NIR) light at 800 nm were employed to increase and decrease conductance, respectively (Figure 2b). The mechanism underlying the light-induced conductance switching was attributed to the ionization of neutral V_Os under short-wavelength light, which reduced the width of the O_D-IGZO/O_R-IGZO interfacial barrier and increased device conductance. In contrast, NIR light irradiation facilitated the neutralization of ionized oxygen vacancies ($V_O{}^{2+}$s), widening the interfacial barrier and decreasing the conductance.

Multiple conductance states with high stability were demonstrated in the AOC memristor, allowing it to mimic the synaptic function of STDP. In one experiment as illustrated in Figure 2c, a single pulse of blue light served as a presynaptic spike, while a train of ten pulses of NIR light acted as postsynaptic spikes. When the presynaptic spike preceded or followed the postsynaptic spike ($\triangle t > 0/\triangle t < 0$), synaptic potentiation or depression occurred ($\triangle W > 0/\triangle W < 0$, W represents the synaptic weight indicated by the device conductance), respectively, with $|\triangle W|$ increasing as $|\triangle t|$ decreased. Further, an experimental demonstration using bilayer IGZO-based AOC memristors showcased a neuromorphic vision sensor with in situ cryptographic computing capability.[157] The sensor demonstrated a wide range of in-sensor operations, including sensing, storage, encryption, decryption, denoising, and destruction of visual images, owing to the unique light wavelength and irradiation history-dependent bidirectional PPC of AOC memristors (Figure 2d). A decrypted image could be encoded and accurately recognized through an AOC memristive neural network. Encrypted and destroyed images could withstand hacking attacks, even with trained neural networks, making the proposed in situ cryptography neuromorphic vision sensor a convenient and effective approach to securing vision information.

Interestingly, a single-layered ZnO memristor with oxide film sputtered in pure argon also exhibited light-tunable conductance changes.[158] These changes were closely associated with the increased or decreased curvature of the conduction band of ZnO upon light irradiation with short or long wavelength (Figure 2e). The implementation of complete Boolean logic functions was realized with this AOC memristor. Figure 2f demonstrates a specific scheme for the Boolean logic "AND" function, where input and output signals were determined based on initial and final conductance states, respectively.

The localized surface plasmon resonance (LSPR) effect enabled the formation of AOC synapses in memristors made of Ag-TiO_2 nanocomposite,[96] as shown in **Figure 3a**. LTP and LTD functions were observed in this LSPR memristor under visible and UV illumination, respectively (Figure 3b,c). The AOC operation of the LSPR memristor resulted from the oxidation and reduction of Ag nanoparticles under illumination with different wavelength light. Under visible light irradiation, Ag nanoparticles were oxidized owing to the LSPR effect, decreasing the Schottky barrier at the Ag/TiO_2 interface and inducing light-induced LTP. Conversely, UV light stimulated the movement of electrons from the valence band to the conduction band of TiO_2, promoting the recombination of electrons with Ag nanoparticles, known as photo-reduction of Ag^+, resulting in light-induced LTD.

In addition to altering the wavelength of incident light, AOC behavior was achieved in memristive devices by adjusting the power density at a constant light wavelength.[159,160] For instance, Chen et al. developed an AOC memristor based on halide perovskites,[159] as shown in Figure 3d. Its conductance could be reversibly modulated by the specific red light (630 nm) of different intensities (11.8 and 0.9 mW cm^{-2}) (Figure 3e). The ionization and neutralization of iodine vacancies (V_Is) were proposed to elucidate the reversible conductance modulation in the perovskite-based AOC memristor. High-power red-light illumination favored the ionization of neutral V_Is, reducing the width of ITO/perovskite interfacial barrier and increasing device conductance. Conversely, under weak light conditions, the neutralization of ionized iodine vacancies ($V_I{}^+$s) dominated, widening the interfacial barrier and decreasing conductance.

A similar example involved an AOC memristor based on silk fibroin protein (MSFP).[160] The structure of the MSFP-based memristor is illustrated in Figure 3f. The positive photoconductance memory (PPM) and negative photoconductance memory (NPM) effects were investigated by applying consecutive light pulses of 405 nm with varying intensities of 80 and 40 mW (Figure 3g), respectively. The reversible alteration of microstructures in the MSFP under different light intensities was crucial for achieving AOC behavior in the device. These light intensity-dependent PPM and NPM effects were utilized for in-sensor image preprocessing, such as image contrast enhancement, noise reduction, and image erasing, eliminating the need for complex processing circuits and analog-to-digital converters (ADCs) between separate sensors and processing units (Figure 3h).

In recent years, AOC memristors have garnered increasing attention from researchers, leading to the development

 © 2024 The Author(s). Advanced Electronic Materials published by Wiley-VCH GmbH

2199160x, 2025, 3, Downloaded from https://advanced.onlinelibrary.wiley.com/doi/10.1002/aelm.202400482 by HONG KONG POLYTECHNIC UNIVERSITY HU NG HOM, Wiley Online Library on [24/02/2026]. See the Terms and Conditions (https://onlinelibrary.wiley.com/terms-and-conditions) on Wiley Online Library for rules of use; OA articles are governed by the applicable Creative Commons License

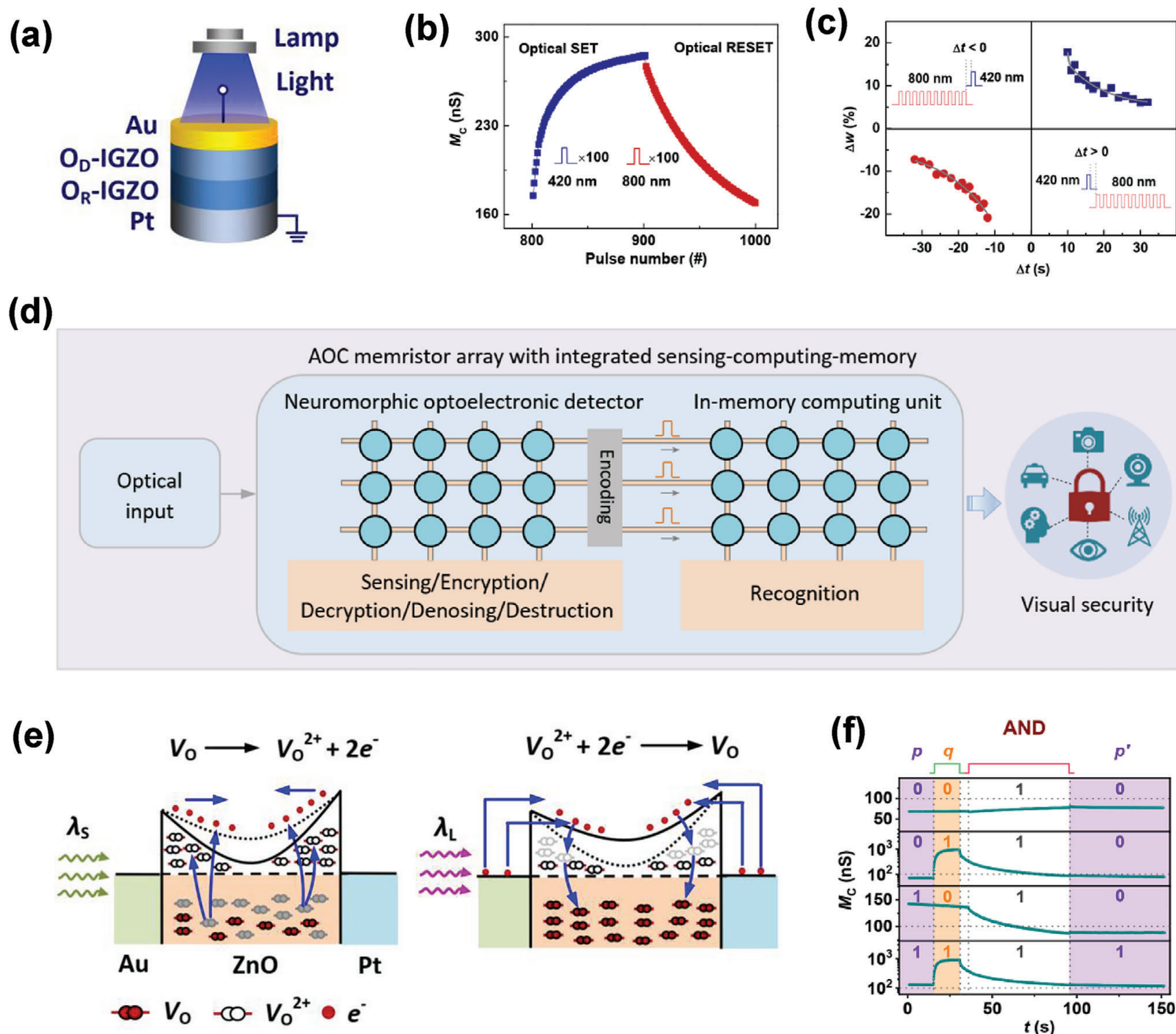

Figure 2. AOC memristors based on IGZO and ZnO. a) Schematic illustration of the O_D-IGZO/O_R-IGZO memristor. b) Reversible conductance regulation under blue and NIR light illumination. c) Emulation of the synaptic STDP. Reproduced with permission.[89] Copyright 2021, The Authors, published by Wiley-VCH under the terms of the Creative Commons Attribution (CC BY) License (a–c). d) In situ cryptography in a neuromorphic vision sensor. The vision sensor consists of two modules: a neuromorphic optoelectronic detector and an in-memory computing unit. Both are constructed using the O_D-IGZO/O_R-IGZO AOC memristors. Reproduced with permission.[157] Copyright 2024, The Authors, published by AIP Publishing under a Creative Commons Attribution (CC BY) license. e) Schematic illustration of ionization and neutralization processes of oxygen vacancies in the ZnO memristor under illumination with short (λ_S) and long (λ_L) wavelength light, respectively. f) Realization of the "AND" logic function. Reproduced with permission.[158] Copyright 2022, The Authors, published by Elsevier under a Creative Commons Attribution (CC BY) license (e,f).

of various AOC memristors based on different materials such as ZnO/Zn_2SnO_4,[161] Ga_2O_3/ZnO,[97] ZnO/MoO_x,[162] NiO/TiO_2,[163] $Cs_2AgBiBr_6$,[164] $MA_{0.4}FA_{0.6}PbI_3$,[165] and NiO–apple pectin.[166]

2.2. Optoelectronic Transistors

The single-transistor synaptic device[167] was initially created in 1996 to simulate the learning function of a synapse. Since then, numerous synaptic transistors have been developed for neuromorphic applications.[26–35,73,168–174] Like optoelectronic memristors, optoelectronic transistors are categorized into two groups: light-electricity synergistic control and all-optical control, based on the weight update method.

2.2.1. Light-Electricity Synergistic Control

The light-electricity synergistic control method often utilizes the PPC effect in optoelectronic transistors to mimic synaptic

© 2024 The Author(s). Advanced Electronic Materials published by Wiley-VCH GmbH

2199160x, 2025, 3, Downloaded from https://advanced.onlinelibrary.wiley.com/doi/10.1002/aelm.202400482 by HONG KONG POLYTECHNIC UNIVERSITY HU NG HOM, Wiley Online Library on [24/02/2026]. See the Terms and Conditions (https://onlinelibrary.wiley.com/terms-and-conditions) on Wiley Online Library for rules of use; OA articles are governed by the applicable Creative Commons License

2199160x, 2025, 3, Downloaded from https://advanced.onlinelibrary.wiley.com/doi/10.1002/aelm.202400482 by HONG KONG POLYTECHNIC UNIVERSITY HU NG HOM, Wiley Online Library on [24/02/2026]. See the Terms and Conditions (https://onlinelibrary.wiley.com/terms-and-conditions) on Wiley Online Library for rules of use; OA articles are governed by the applicable Creative Commons License

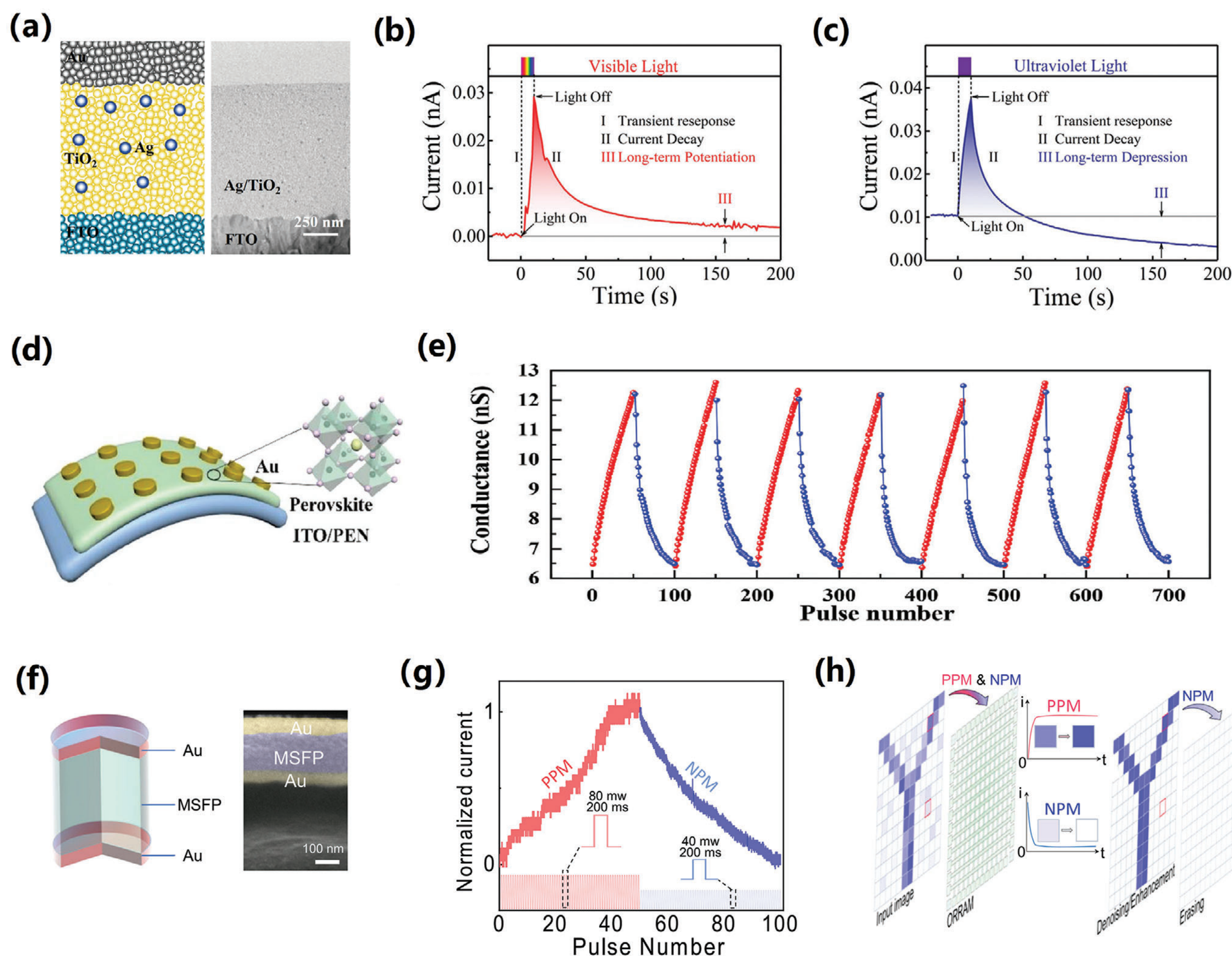

Figure 3. AOC memristors based on Ag–TiO_2, perovskite, and MSFP. a) Schematic illustration of the memristor using an Ag nanoparticle–TiO_2 nanocomposite film. b,c) Synaptic LTP (b) and LTD (c) under visible and UV light. Reproduced with permission.[96] Copyright 2022, The Authors, published by Wiley-VCH under a Creative Commons Attribution (CC BY) license (a–c). d) Schematic illustration of the Au/perovskite/ITO/PEN memristor. e) Reversible modulation of conductance under red light (630 nm) illumination. LTP and LTD are implemented at light power intensities of 11.8 and 0.9 mW cm^{-2}, respectively. Reproduced with permission.[159] Copyright 2023, Wiley-VCH (d,e). f) Schematic illustration of the MSFP-based memristor. g) Reversible modulation of conductance under blue light (405 nm) illumination. LTP and LTD are realized at light power intensities of 80 and 40 mW cm^{-2}, respectively. h) Image contrast enhancement, denoising and erasing. Reproduced with permission.[160] Copyright 2023, The Authors, published by Springer Nature under a Creative Commons Attribution 4.0 International License (f–h).

LTP behavior.[92,168,175] By adjusting the gate voltage, the PPC of the device can be effectively eliminated, allowing the simulation of synaptic LTD.[92,169,170,173] Various photosensitive materials, such as oxide semiconductors,[168,175–188] 2D materials,[189–194] perovskites,[93,195–200] and organic materials,[201–207] have been employed as channel materials in optoelectronic transistors. The synaptic weights of these devices are updated through a combination of light and electricity signals.

Park and co-workers developed a TiO_2/IGZO heterojunction synaptic transistor[176] for optoelectronic neuromorphic computing (**Figure** 4a,b). By adding a TiO_2 layer on IGZO, the device's response wavelength range was extended to red light, enhancing photoresponsivity and enabling pronounced PPC behavior across the visible light spectrum. The device exhibited good retention characteristics in photoconductance with a negative gate bias, while a positive gate bias effectively eliminated the PPC effect and reduced the device conductance. As depicted in Figure 4c, LTP was induced by green light pulses at a frequency of 2 Hz, while LTD was induced by positive gate pulses with an amplitude of 6 V.

Currently, achievements in optoelectronic synapse primarily focus on UV or visible-sensitive materials with relatively large bandgaps.[70] Reports on synaptic transistors with NIR sensitivity are limited, mainly due to the inferior NIR sensitivity of materials caused by the bandgap limitation.[155] To address this issue, an optoelectronic transistor based on a $MoSe_2/Bi_2Se_3$ heterojunction[208] was demonstrated to mimic synaptic plasticity using NIR light stimuli. The device structure is illustrated in Figure 4d. In this device, the p-type pentacene and $MoSe_2/Bi_2Se_3$/polymethyl methacrylate (PMMA) composite film

© 2024 The Author(s). Advanced Electronic Materials published by Wiley-VCH GmbH

2199160x, 2025, 3, Downloaded from https://advanced.onlinelibrary.wiley.com/doi/10.1002/aelm.202400482 by HONG KONG POLYTECHNIC UNIVERSITY HU NG HOM, Wiley Online Library on [24/02/2026]. See the Terms and Conditions (https://onlinelibrary.wiley.com/terms-and-conditions) on Wiley Online Library for rules of use; OA articles are governed by the applicable Creative Commons License

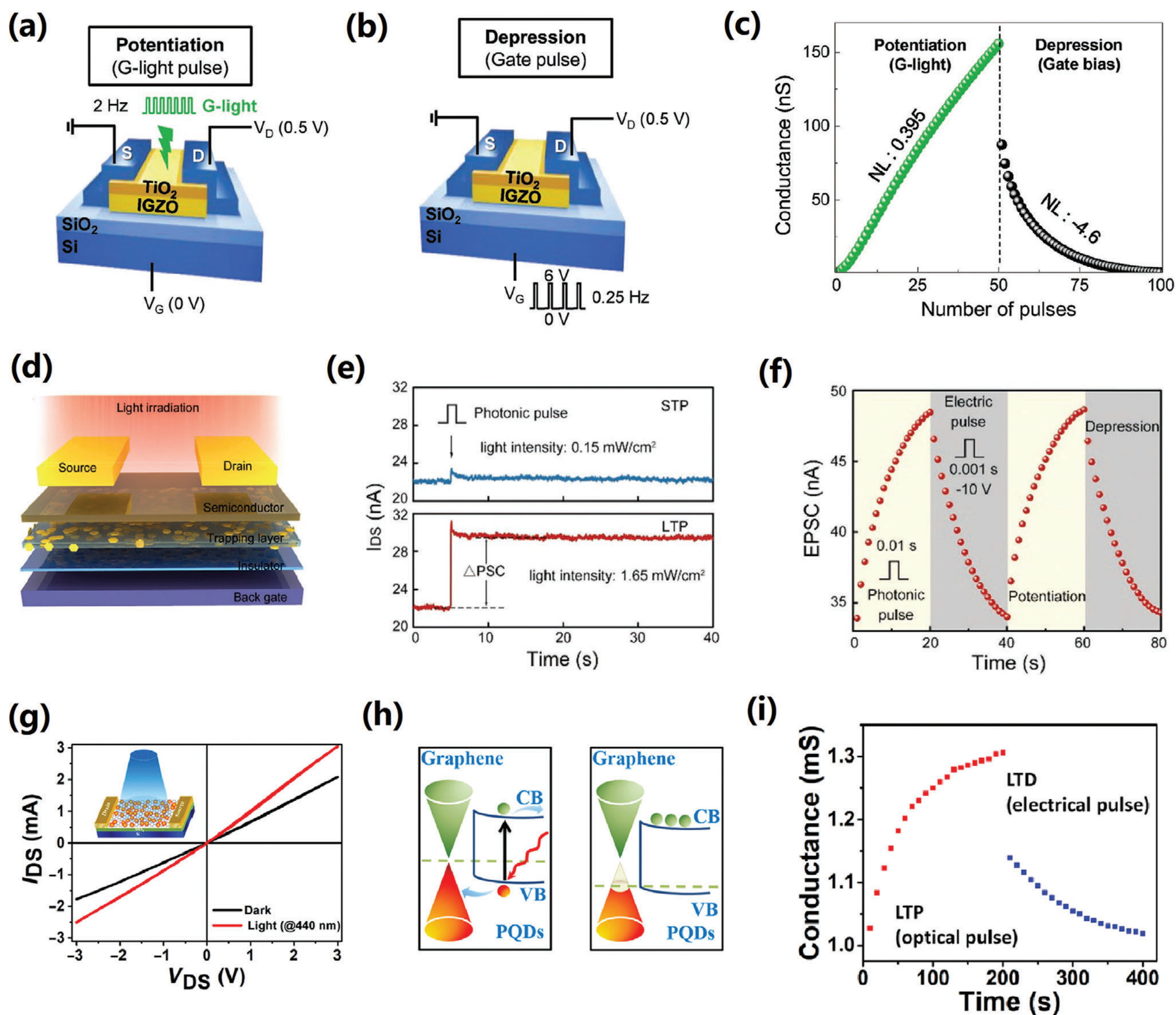

Figure 4. Light-electricity synergistically controlled transistors. a,b) Schematic illustrations of implementation schemes of optical potentiation (a) and electrical depression (b) in the TiO_2/IGZO transistor. c) Reversible conductance regulation. Reproduced with permission.[176] Copyright 2023, Wiley-VCH (a–c). d) Device structure of the $MoSe_2/Bi_2Se_3$ transistor. e) STP and LTP under NIR light (790 nm) irradiation with different power intensities (upper panel, 0.15 mW cm^{-2}; lower panel, 1.65 mW cm^{-2}). f) Reversible modulation of conductance upon optical and electrical stimulation. Reproduced with permission.[208] Copyright 2020, Wiley-VCH (d–f). g) Drain current (I_{DS}) versus drain voltage (V_{DS}) characteristics of the G-PQD transistor with and without blue light (440 nm) illumination. h) Energy level diagrams of the G-PQD structure in photoexcitation (left panel) and photogating (right panel) processes. i) LTP under light illumination at positive drain voltage and LTD upon negative drain voltage. Reproduced with permission.[93] Copyright 2020, The Authors, published by AAAS Science under a Creative Commons Attribution NonCommercial License 4.0 (CC BY-NC) (g–i).

served as the channel material and photosensitive charge trapping layer, respectively. Under NIR light illumination at a wavelength of 790 nm, the $MoSe_2/Bi_2Se_3$/PMMA layer demonstrated electron-trapping ability, resulting in an increase in the conductivity of the channel material. As illustrated in Figure 4e, the power intensity-dependent STP and LTP behaviors were investigated using a single NIR light pulse with intensities of 0.15 and 1.65 mW cm^{-2}, respectively. Negative electric pulses applied to the back gate released these trapped electrons, thereby decreasing the device's conductance. LTP and LTD were realized by applying photonic and electric pulses successively, as shown in Figure 4f. Similar NIR-triggered synaptic behaviors were also observed in transistors based on PbS-QDs/PMMA,[209] IGZO/Ag_2O,[210] B-doped Si nanocrystals/WSe_2,[211] upconverting nanoparticles-MoS_2,[212] InGaCdO,[213] MoS_2/PbS,[214] and IR-780 iodide/PMMA/pentacene.[215]

In addition to adjusting the gate voltage, the drain-source voltage could also be modified to regulate the conductance of synaptic transistors. Thomas et al. demonstrated an optoelectronic transistor based on perovskite quantum dots (PQDs) and graphene (Gr)[93] to achieve reversible regulation of device conductance through light and varying drain-source voltages.

 © 2024 The Author(s). Advanced Electronic Materials published by Wiley-VCH GmbH

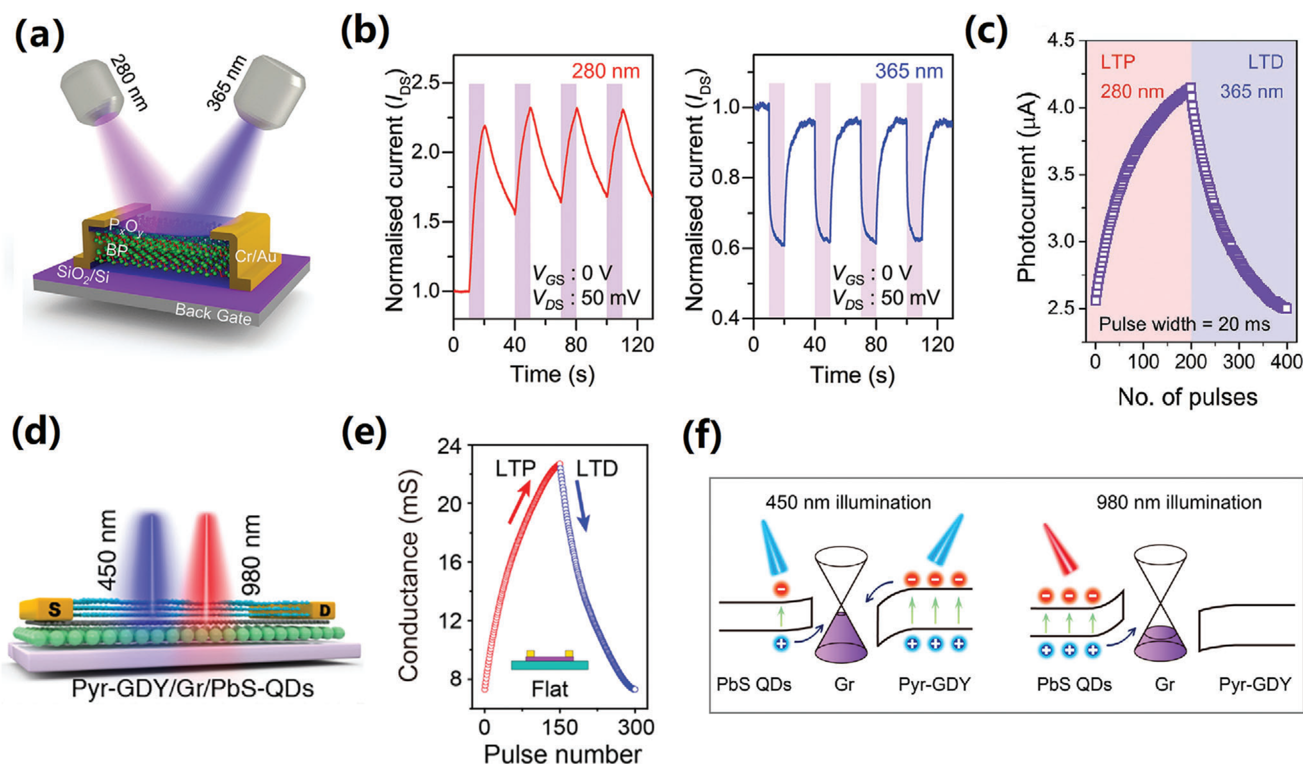

Figure 5. AOC transistors. a) Schematic illustration of the BP transistor. b) Normalized transient photocurrent under 280 nm (left panel) and 365 nm (right panel) illumination, measured at a constant drain voltage of 50 mV. c) LTP under 280 nm pulses and LTD under 365 nm pulses. Reproduced with permission.[216] Copyright 2021, Wiley-VCH (a–c). d) Schematic illustration of the transistor based on a Pyr-GDY/Gr/PbS QD heterostructure. e) LTP under 980 nm pulses and LTD under 450 nm pulses. f) Energy band diagrams under 450 and 980 nm light illumination. Reproduced with permission.[217] Copyright 2021, American Chemical Society (d–f).

Figure 4g illustrates the current–voltage characteristics of the device in darkness and under blue light illumination, revealing a significant current increase under light. Figure 4h depicts the energy band diagram of the device, showing an interfacial barrier between Gr and the PQDs that created a built-in electric field directed from the PQDs to Gr. Under illumination, the photogenerated electrons and holes in PQDs were effectively dissociated at the Gr/PQDs interface by the built-in field. The holes were transported to the Gr from PQDs, resulting in an increase in device current. Meanwhile, the electrons were trapped in the PQDs, inducing a photogating effect as electrons accumulated. By applying a negative drain-source voltage, the photogenerated carriers trapped in the PQDs were released, decreasing the device conductance. Consequently, synaptic LTP/LTD behaviors were demonstrated by applying optical and electrical pulses at the drain (Figure 4i).

2.2.2. All-Optical Control

All-optical control in optoelectronic transistors enables the reversible adjustment of synaptic weights without the need for electrical inputs. For instance, an AOC transistor was developed based on vertically-stacked black phosphorus (BP) layers,[216] as illustrated in **Figure** 5a, taking advantage of the positive and negative photoresponses induced by defects in black phosphorus BP. The normalized transient photoresponse of BP devices under 280 and 365 nm wavelength illumination pulses is depicted in Figure 5b. These responses were obtained at a constant drain-source voltage with no gate voltage (V_G = 0 V). Irradiation with 280 nm UV light increased the device conductance, associated with the positive photocurrent during optical SET, caused by the trapping of photoexcited carriers. Conversely, irradiation with 365 nm UV light decreased the conductance due to the trapping of photoexcited charge carriers at localized defect sites induced by surface oxidation of the BP flake. Synaptic LTP and LTD functions were realized in this BP device through successive light illuminations of 280 and 365 nm (Figure 5c).

Similarly, a pyrenyl graphdiyne (Pyr-GDY)/Gr/PbS-QD heterostructure[217] was proposed for synaptic transistors with AOC characteristics (Figure 5d). Conductance increases and decreases were achieved by irradiating the device with 980 and 450 nm light, respectively, without the need for a gate voltage. The AOC mechanism is illustrated in Figure 5e. When illuminated with 450 nm light, the Pyr-GDY film absorbed most of the light, generating electron–hole pairs. The photogenerated electrons moved to Gr due to the built-in electric field between Pyr-GDY and Gr, while the holes remained trapped in Pyr-GDY (Figure 5f), inducing a positive photogating effect that decreased the device conductance. Conversely, under 980 nm light illumination, PbS QDs served as the primary light-absorbing layer, with photogenerated holes transferring to the Gr channel and

© 2024 The Author(s). Advanced Electronic Materials published by Wiley-VCH GmbH

2199160x, 2025, 3, Downloaded from https://advanced.onlinelibrary.wiley.com/doi/10.1002/aelm.202400482 by HONG KONG POLYTECHNIC UNIVERSITY HU NG HOM, Wiley Online Library on [24/02/2026]. See the Terms and Conditions (https://onlinelibrary.wiley.com/terms-and-conditions) on Wiley Online Library for rules of use; OA articles are governed by the applicable Creative Commons License

trapped electrons remaining in the PbS QDs, increasing the device conductance.

In addition to relying on the wavelength and intensity of irradiated light,[218–227] AOC synapse behaviors have been achieved with the assistance of gate voltage in optoelectronic transistors using various materials, including metal oxides,[228] 2D materials,[229–239] electrostatically doped Si,[240] and organic compounds.[241] For instance, Zhou and co-workers developed a BP/Al_2O_3/WSe_2/h-BN heterojunction optoelectronic transistor for a neuromorphic visual sensor,[237] demonstrating non-volatile positive and negative photocurrents by changing the gate voltage polarity. When a positive gate voltage was applied, photoelectrons in the WSe_2 tunneled through the *h*-BN and flowed into the metal gate, with the remaining holes enhancing the channel current and leading to a high conductance state. When a negative gate voltage was applied, the stored holes absorbed photon energy to leap the WSe_2/*h*-BN interface barrier, reducing the stored holes and decreasing the channel current, corresponding to a low conductance state.

2.3. Other Optoelectronic Synapse Devices

In addition to memristors and transistors, some two-terminal[128,242–254] and three-terminal[72,255] heterogeneous structures have been reported for optoelectronic synapses. Lv et al. developed an AOC synaptic device based on an amorphous ZnAlSnO/SnO p–n heterojunction[242] to mimic excitatory and inhibitory synaptic behaviors (**Figure 6**a). Red light (635 nm) was utilized to simulate LTP, while green light (532 nm) was employed for LTD simulation, as depicted in Figure 6b,c. The high sensitivity of amorphous oxide semiconductors to visible light, attributed to abundant defects like V_Os, was leveraged in this device. By irradiating ZnAlSnO with 635 nm light, V_Os were ionized, generating photogenerated electrons and leading to an increase in device conductance, corresponding to LTP behavior. Conversely, irradiating with green light caused the electrons in the conduction band of ZnAlSnO to absorb sufficient energy to cross the interface potential barrier to SnO, resulting in a decrease in device conductance and, consequently, LTD.

Based on the lateral Bi_2O_2Se/Gr hybrid structure, a three-terminal photodetector[255] was proposed to implement the LTP/LTD function utilizing optical signals, as illustrated in Figure 6d. Upon illumination at 635 nm, the photoconductive and bolometric effects induced a positive photoresponse in the Bi_2O_2Se device (Figure 6e). In contrast, illumination at 365 nm led to a negative photoresponse in the Gr device (Figure 6f) due to UV-induced desorption of oxygen or water molecules from the Gr surface, which reduced the concentration of hole carriers in Gr. Thus, synaptic LTP and LTD functions were achieved by utilizing the positive and negative photoresponses induced by 635 and 365 nm light, respectively.

The combination of photosensitive devices with electronic synapses offers another method for implementing optoelectronic synapses.[72,256–261] Yang et al. developed a synaptic device known as one-phototransistor–one-memristor (1PT1R),[256] as illustrated in Figure 6g. The 1PT1R synaptic device was constructed using light-programmable ZnO thin-film transistors (TFTs) and nonvolatile Mo/SiO_2/W memristors. The Mo/SiO_2/W memristor stored and processed optical signals from the phototransistor, acting as a nonvolatile component in the 1PT1R structure. Figure 6h shows a plot of the typical current–voltage curves of the Mo/SiO_2/W device in 100 consecutive DC sweeps. The light-tunable switching characteristics of the 1PT1R devices were evaluated by applying positive voltage pulses for potentiation under light illumination from 1.25 to 2.5 mW μm^{-2}, followed by negative voltage pulses for depression with illumination from 2.5 to 1.25 mW μm^{-2}. These 1PT1R devices demonstrated highly linear weight adjustments through light programming, as depicted in Figure 6i.

Table 1 presents a detailed comparison of optoelectronic synapses based on different operation modes, focusing on active layer material, synaptic function, light power intensity, on/off ratio, and the linearity of conductance changes. Several crucial aspects require focused efforts in future research. First, the table indicates that oxide semiconductors are the primary materials for constructing optoelectronic synapses. However, oxide semiconductors typically have a wide bandgap, limiting their response to visible and NIR light. Combining oxide semiconductors with narrow bandgap materials is an effective approach to expand the wavelength range of device light response. Second, for most devices, light-induced LTP can be achieved based on the PPC effect, whereas LTD can only be obtained through applying electrical signals. Light-electricity synergistic control may increase operational complexity and impact device stability. AOC devices can effectively avoid the detrimental influence of large electrical signals and Joule heating on their microstructure, thereby enhancing their stability. Third, light power density required for optoelectronic synapses is generally in the order of mW cm^{-2}, resulting in significant energy consumption. Enhancing the photoresponsivity of materials via defect control, element doping, and other methods, along with rational device structure design (such as constructing type II heterojunctions), can help lower energy consumption. Fourth, further efforts are required to improve the range and linearity of conductance changes in optoelectronic synapses. The weak photoelectric response and poor retention of light-induced conductance states are the main limiting factors for increasing the device's conductance change window. Research on photosensitive materials and device structures remains an important future direction. In addition, the linearity of conductance changes can be significantly improved by optimizing the application scheme of optical signals.

3. Optoelectronic Neurons

Artificial neurons are nonlinear processing units capable of spatially and temporally integrating input signals from numerous synapses. Compared to biological synapses, more complex dynamic behaviors are demonstrated by biological neurons. Traditionally, artificial neurons have been constructed using CMOS circuits with multiple active components.[59] However, a recent shift has occurred toward utilizing emerging electronic devices such as threshold switching (TS) memristors,[17–21,262–264] phase-change devices,[38,39] spintronic devices,[50,265] and transistors[32,85,266–268] to function as artificial neurons. These devices have successfully replicated basic neuronal functions through electrical stimulation, including leaky

© 2024 The Author(s). Advanced Electronic Materials published by Wiley-VCH GmbH

2199160x, 2025, 3, Downloaded from https://advanced.onlinelibrary.wiley.com/doi/10.1002/aelm.202400482 by HONG KONG POLYTECHNIC UNIVERSITY HU NG HOM, Wiley Online Library on [24/02/2026]. See the Terms and Conditions (https://onlinelibrary.wiley.com/terms-and-conditions) on Wiley Online Library for rules of use; OA articles are governed by the applicable Creative Commons License

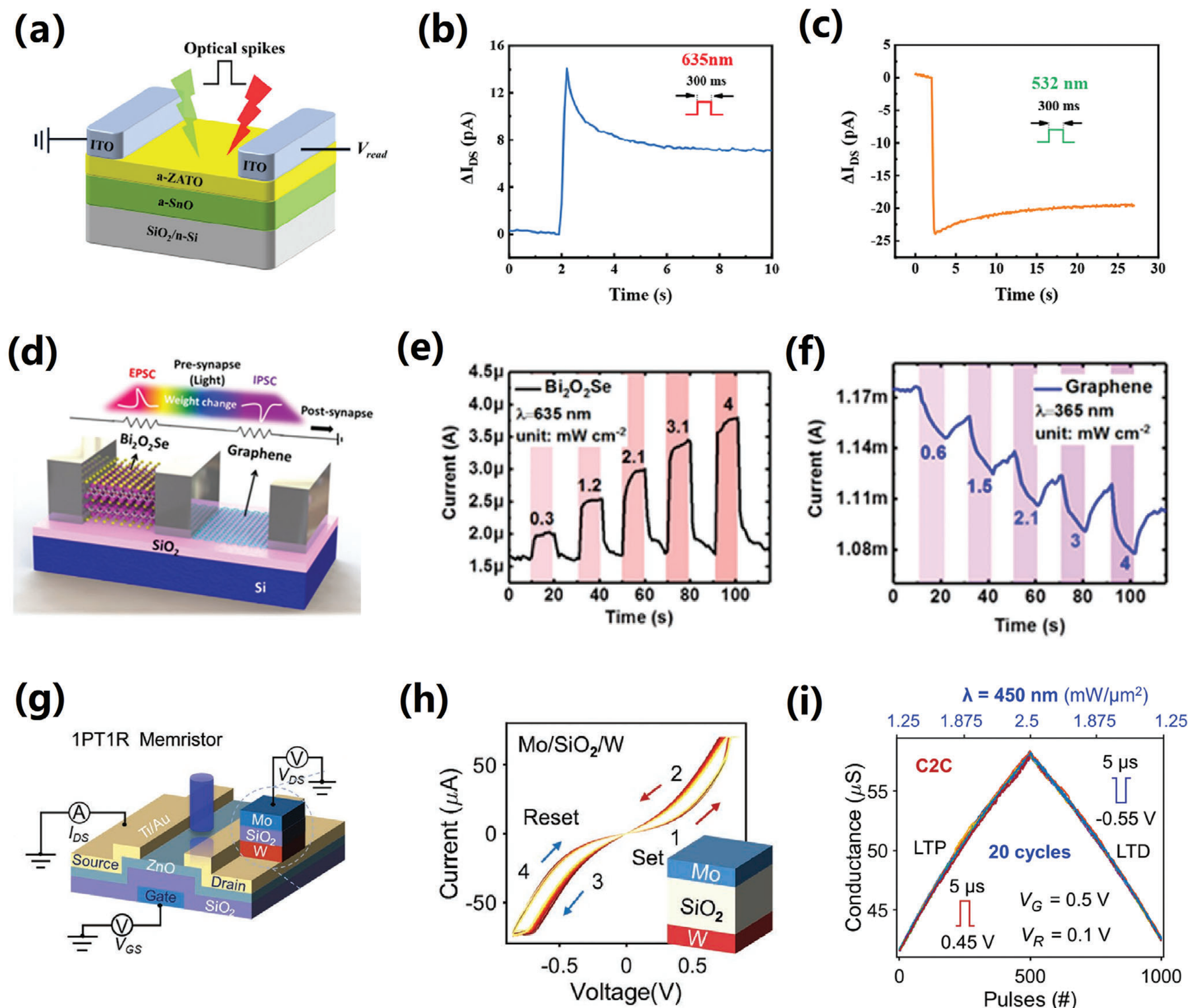

Figure 6. Optoelectronic synapse devices based on two-terminal and three-terminal heterogeneous structures. a) Device structure of the ZnAlSnO/SnO AOC synapse. b,c) Emulation of LTP under red light (635 nm) illumination (b) and LTD under green light (532 nm) illumination (c). Reproduced with permission.[242] Copyright 2024, Wiley-VCH (a–c). d) Schematic illustration of the optoelectronic device with a Bi_2O_2Se/Gr hybrid structure. e,f) Positive (e) and negative (f) photoresponse upon illumination at 635 and 365 nm. Reproduced with permission.[255] Copyright 2020, Wiley-VCH (d–f). g) Schematic illustration of the synaptic device based on a one ZnO-phototransistor and one SiO_2-memristor (1PT1R) structure. h) *I–V* characteristics of the Mo/SiO_2/W memristor. i) LTP and LTD behaviors of the 1PT1R device. Conductance increases with positive electric pulses and enhanced light illumination. Conversely, conductance decreases with negative electric pulses and weakened light illumination. Reproduced with permission.[256] Copyright 2023, Wiley-VCH (g–i).

integrate-and-firing (LIF),[18,19,38,39] threshold-driven firing,[18,19,32] and all-or-nothing behaviors.[17,19,266] The development of optoelectronic neurons has introduced advantages such as lower power consumption and higher efficiency, expanding the applications of electronic neurons to optoelectronic neuromorphic computing and visual function simulation. Despite these potential benefits, research on optoelectronic neurons lags behind optoelectronic synaptic devices due to their intricate dynamic behaviors.[59] Most optoelectronic neurons can be categorized into two types based on the device used: threshold switch neurons and semiconductor laser neurons.

3.1. Threshold Switch Neurons

Optoelectronic neurons, combining photosensitive and electronic threshold switch devices, have been developed.[22,78,269–271] For instance, Wang et al. fabricated an artificial sensory neuron with a Ta/$IGZO_4$/Pt sensor for tunable light response and a Pt/NbO_x/Ta-based Mott memristor,[78] as depicted in **Figure 7a**. The $IGZO_4$ device exhibited excellent UV sensing capabilities, with resistance decreasing as the wavelength decreased. The TS characteristics of the NbO_x device were utilized to mimic oscillatory behavior in the neuron. Consequently, the integrated sensory

 © 2024 The Author(s). Advanced Electronic Materials published by Wiley-VCH GmbH

2199160x, 2025, 3, Downloaded from https://advanced.onlinelibrary.wiley.com/doi/10.1002/aelm.202400482 by HONG KONG POLYTECHNIC UNIVERSITY HU NG HOM, Wiley Online Library on [24/02/2026]. See the Terms and Conditions (https://onlinelibrary.wiley.com/terms-and-conditions) on Wiley Online Library for rules of use; OA articles are governed by the applicable Creative Commons License

2199160x, 2025, 3, Downloaded from https://advanced.onlinelibrary.wiley.com/doi/10.1002/aelm.202400482 by HONG KONG POLYTECHNIC UNIVERSITY HU NG HOM, Wiley Online Library on [24/02/2026]. See the Terms and Conditions (https://onlinelibrary.wiley.com/terms-and-conditions) on Wiley Online Library for rules of use; OA articles are governed by the applicable Creative Commons License

Table 1. Comparison of emerging optoelectronic synapses.

Device type	Active layer	Operating mode	Operating wavelength [nm]	Power density [mW cm^{-2}]	On/off ratio	Nonlinearity	Ref.
Memristor	ZnO_{1-x}/AlO_y	LESC	310	0.072	≈3	–	[90]
	In_2O_3/ZnO	LESC	365	0.4	≈2	–	[101]
	ZnO/HfO_x	LESC	365	5.11	≈10	0.469	[115]
	NiO/ZnO	LESC	350	0.038	≈3	–	[119]
	MoO_x	LESC	365	0.88	≈2	–	[116]
	MoS_2	LESC	310	0.11	≈7	–	[91]
	O_D-IGZO/O_R-IGZO	AOC	420/800	0.02/0.024	≈2	–	[89]
	Ag–TiO_2	AOC	365/532	3.7/21.8	≈10	–	[96]
	ZnO	AOC	530/650	0.036	≈4	–	[158]
	ZnO/Zn_2SnO_4	AOC	405/633	40/55	≈1.09	4.86/3.58	[161]
	Perovskite	AOC	630	0.9/11.8	≈2	–	[159]
	Silk fibroin protein	AOC	405	80/40	≈2	–	[160]
Transistor	TiO_2/IGZO	LESC	520	4.88	>150	0.395	[176]
	IGZO	LESC	405	0.182	>10	–	[180]
	VO_2	LESC	375	84	≈1.8	0.2	[187]
	NbS_2/MoS_2	LESC	532	0.0031	≈6	0.65	[173]
	Perovskite	LESC	440	0.001	≈1.3	–	[93]
	BP	AOC	280/365	3.5/7.3	≈1.7	≈2.7/3	[216]
	Pyr-GDY/Gr/PbS-QD	AOC	450/980	10/150	≈3	1.7/1.9	[217]
	Gr/TiO_2-QD	AOC	365/635	0.1/26	≈1.03	–	[218]
	In_2O_3/Al_2O_3/Y6	AOC	365/808	0.8/1.7	>5	≈1.6/0.7	[222]
Others	MoS_2	LESC	550	23.6	≈1.1	–	[251]
	ZnAlSnO/SnO	AOC	405/635	0.033/0.015	≈2.7	–	[242]
	Si doped β-Ga_2O_3/ZnO	AOC	255/370	0.17/1.22	≈4	0.05/0.04	[244]

neuron was capable of directly responding to UV light and producing consistent electrical spikes. As illustrated in Figure 7b, the sensory neuron showed four stable oscillation frequencies in response to different light inputs: a dark state, 365 nm, 254 nm, and simultaneous illumination of 365 and 254 nm light. These distinct oscillation frequencies in response to different UV input signals suggested the potential for detecting and converting UV images encoded with varying wavelengths.

Similarly, a vertically integrated optoelectronic neuron[22] was demonstrated, which was capable of converting visible light into spike trains and distinguishing lights of different wavelengths. The device was structured vertically with ITO/Ta_2O_5/Ag/IGZO/ITO (Figure 7c). In this device, the ITO/Ta_2O_5/Ag-based TS memristor functioned as an artificial spike-encoder, while the Ag/IGZO/ITO-based photoresistor acted as a photoreceptor. The photoreceptors converted light into electrical signals that acted on the TS memristor to control the firing frequency of neurons. Initially, the neuron remained inactive in a dark environment. Under irradiation, the persistent light was transformed into spike trains with a specific frequency level, as depicted in Figure 7d. The frequency of the output spikes in the neuron had been shown to positively correlate with both the intensity and wavelength (Figure 7e). Within a certain range of densities, there was no overlap in the frequency responses to wavelengths of 360, 405, and 532 nm, allowing the firing frequency to convey the color and intensity details of the light stimulus.

In addition, it is worth noting that optoelectronic neurons based on a single device have been demonstrated, including Si phototransistor,[85] ZnO/Sb-doped-SnO_2/fluorine-doped-tin-oxide (FTO) device,[77] MoS_2 phototransistor,[272] and black phosphorous (BP)-$CsPbBr_3$ TS memristor.[273] For example, Chai et al. developed an optoelectronic graded neuron based on a MoS_2 phototransistor for bioinspired in-sensor motion perception,[272] as illustrated in Figure 7f. Under red light (660 nm) illumination, the drain current (I_d) of the MoS_2 phototransistor significantly increased (Figure 7g). Subsequently, the I_d gradually decreased to zero post-illumination due to the release of charges from the shallow trapping centers. As the time interval between consecutive light pulses increased, the responses to the light pulses became almost independent. However, after four consecutive stimulation pulses with shorter time intervals, the phototransistor effectively integrated the light stimuli through nonlinear accumulation, mimicking the properties of graded neurons. The distinct responses to the various four-frame actions, as shown by the exported I_d under four light pulses (16 combinations) with a shorter time interval in Figure 7h, indicated the device's ability to temporally encode four-pulse light stimulation, similar to graded neurons. Based on the photoelectric characteristics described above, the MoS_2 phototransistor could directly identify various types of motion at sensory terminals, mimicking the non-spiking graded neurons of insect vision systems.

© 2024 The Author(s). Advanced Electronic Materials published by Wiley-VCH GmbH

2199160x, 2025, 3, Downloaded from https://advanced.onlinelibrary.wiley.com/doi/10.1002/aelm.202400482 by HONG KONG POLYTECHNIC UNIVERSITY HU NG HOM, Wiley Online Library on [24/02/2026]. See the Terms and Conditions (https://onlinelibrary.wiley.com/terms-and-conditions) on Wiley Online Library for rules of use; OA articles are governed by the applicable Creative Commons License

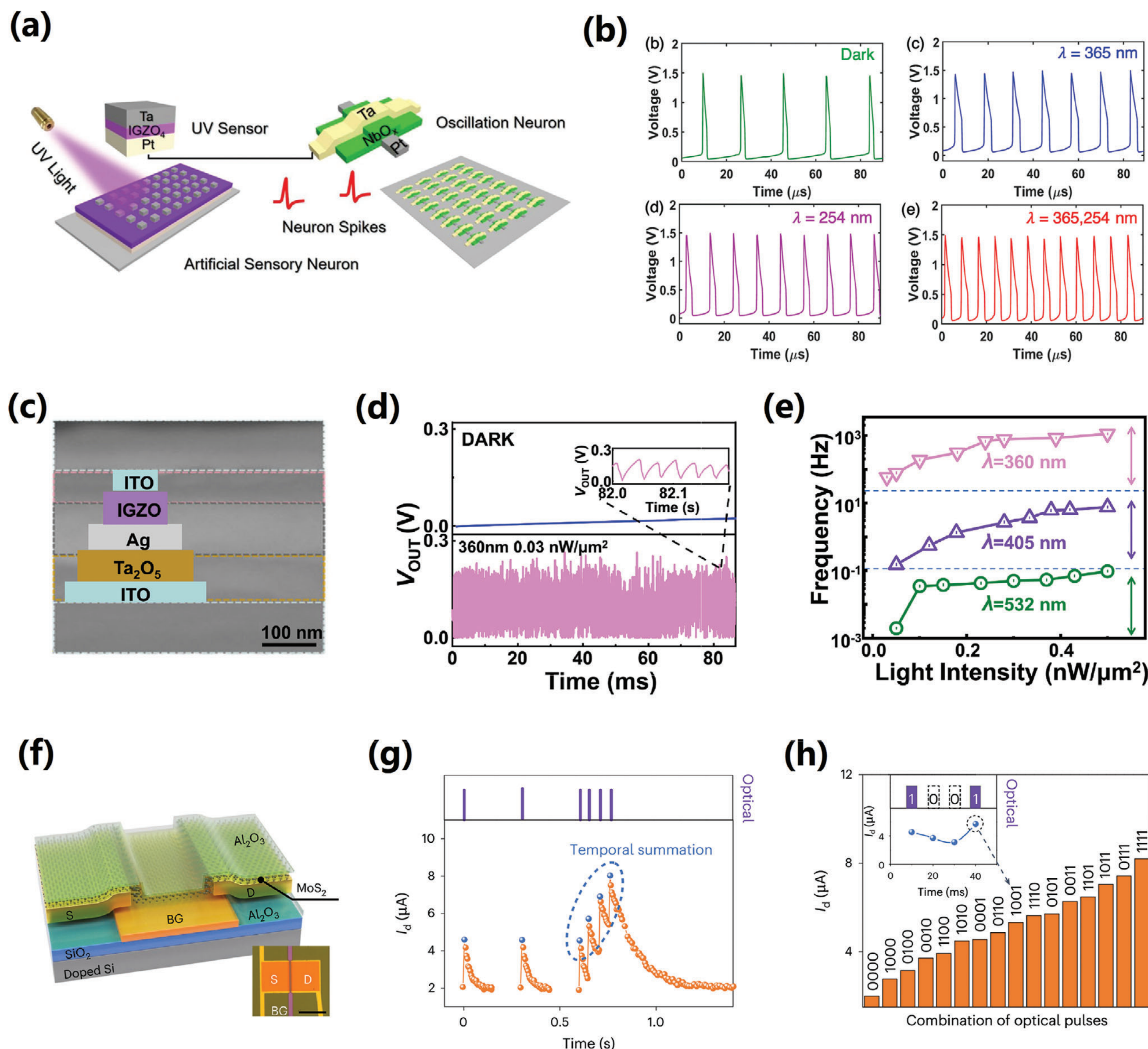

Figure 7. Threshold switch neurons. a) Schematic images of the artificial visual sensory neuron consisting of an $IGZO_4$ UV sensor and a NbO_x oscillation neuron. b) Firing frequencies of the visual sensory neuron with and without UV illumination. Reproduced with permission.[78] Copyright 2020, American Chemical Society (a,b). c) Sectional view of the vertically integrated ITO/Ta_2O_5/Ag/$IGZO_4$/ITO neuron. d) Firing behaviors in dark and under 360 nm illumination. e) Firing frequencies under 360, 405, and 532 nm illumination with different light intensities. Reproduced with permission.[22] Copyright 2023, The Authors, published by Springer Nature under a Creative Commons Attribution 4.0 International License (c–e). f) Schematic illustration of the optoelectronic graded neuron based on a MoS_2 transistor. g) Photocurrent response of the MoS_2 transistor. h) Photocurrent response under four-bit light pulses. The inset illustrates the encoding process for '1001', with '1' and '0' denoting with and without light illumination, respectively. Reproduced with permission.[272] Copyright 2023, The Authors, under exclusive license to Springer Nature Limited (f–h).

3.2. Semiconductor Laser Neurons

Among semiconductor lasers, vertical-cavity surface-emitting lasers (VCSELs) offer significant advantages, including low cost, small footprint, high-speed operation, and a wide range of neuron-like dynamics, making them well-suited for laser neurons.[274–280] VCSELs demonstrate behaviors similar to those of biological neurons, such as thresholding dynamics, phasic and tonic spiking regimes, and spike bursting.[274]

Hurtado et al. developed a LIF spiking photonic neuron based on VCSELs for performing pattern recognition tasks at ultrafast sub-ns rates with continuous operation.[275] **Figure 8a** illustrates the experimental setup of a spiking VCSEL-neuron under external optical injection. A tunable laser (TL) was used to generate constant optical signals with a wavelength of 1300 nm. These optical signals were sequentially passed through an isolator (ISO), a variable optical attenuator (VOA), and polarization controllers (PC) to control the power and polarization, before being encoded

 © 2024 The Author(s). Advanced Electronic Materials published by Wiley-VCH GmbH

2199160x, 2025, 3, Downloaded from https://advanced.onlinelibrary.wiley.com/doi/10.1002/aelm.202400482 by HONG KONG POLYTECHNIC UNIVERSITY HU NG HOM, Wiley Online Library on [24/02/2026]. See the Terms and Conditions (https://onlinelibrary.wiley.com/terms-and-conditions) on Wiley Online Library for rules of use; OA articles are governed by the applicable Creative Commons License

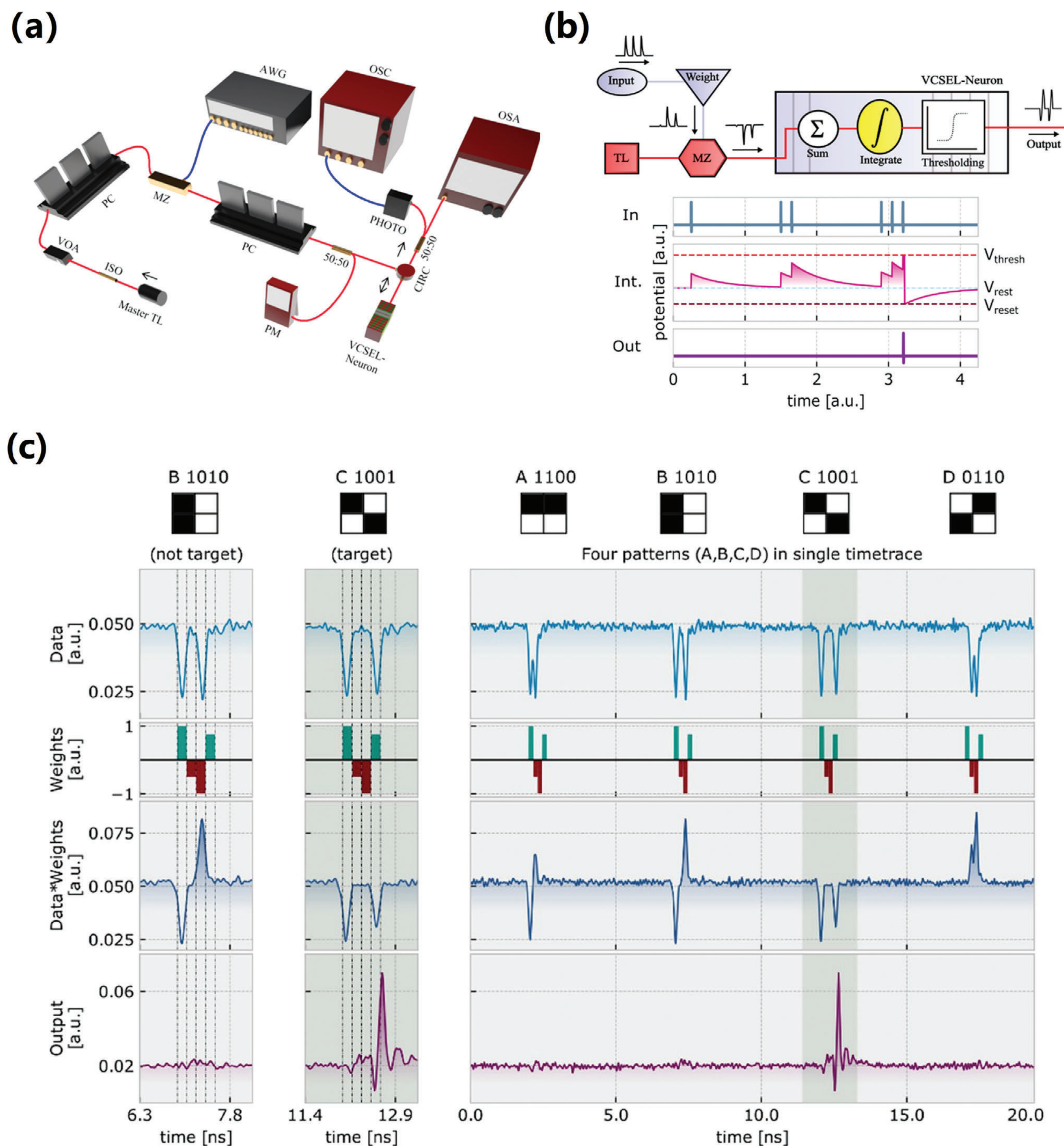

Figure 8. VCSEL neuron. a) Experimental setup of the VCSEL neuron system. Optical fiber connections are indicated in red, while electrical connections are indicated in blue. b) Flow diagram of the VCSEL neuron. When the threshold requirement is fulfilled, the system fires a spike. c) Pattern recognition. Reproduced with permission.[275] Copyright 2020, The Authors. Published by Springer Nature under a Creative Commons Attribution 4.0 International License.

using a Mach–Zehnder (MZ) amplitude modulator and an arbitrary waveform generator (AWG). The optical line was divided into two paths via a 50:50 fiber directional coupler. One path was linked to a power meter (PM) to monitor the injected intensity, while the other was linked to an optical circulator (CIRC) that injected the optical signals into the VCSEL-neuron. The VCSEL-neuron's output was collected with a photodetector, a real-time oscilloscope, and an optical spectrum analyzer. These input stimuli were summed and integrated by the VCSEL-neuron, which then fired a spike upon exceeding the threshold energy for spike

 © 2024 The Author(s). Advanced Electronic Materials published by Wiley-VCH GmbH

2199160x, 2025, 3, Downloaded from https://advanced.onlinelibrary.wiley.com/doi/10.1002/aelm.202400482 by HONG KONG POLYTECHNIC UNIVERSITY HU NG HOM, Wiley Online Library on [24/02/2026]. See the Terms and Conditions (https://onlinelibrary.wiley.com/terms-and-conditions) on Wiley Online Library for rules of use; OA articles are governed by the applicable Creative Commons License

Table 2. Comparison of optoelectronic neurons.

Device type	Active layer	Neuronal functions	Operating wavelength [nm]	Frequency [Hz]	Energy consumption	Ref.
Memristor	NbO_x	Oscillation	254/365	≈100 K	–	[78]
	Ta_2O_5	Oscillation	360/405/532	≈1.2 K	≈40 pJ	[22]
	BP–$CsPbBr_3$	LIF	365/450/520	>2.5	≈20.3 nJ	[273]
	NbO_x	LIF	365	≈1.85 M	≈1.06 nJ	[271]
	SiO_2	LIF	808	≈30	–	[215]
Transistor	Si	LIF	405/520/638	≈60	≈6.86 nJ	[85]
	Al_2O_3	LIF	532	≈60	≈20 pJ	[269]
	MoS_2	Graded neurons	660	≈100	–	[272]

activation (Figure 8b). Figure 8c demonstrates the recognition of target 4-bit data patterns, where the 4-bit patterns were weighted before being injected into the VCSEL-neuron, which produced a spike only in response to the target pattern, remaining silent for non-target patterns.

In addition, VCSEL-neurons exhibited both excitatory and inhibitory spiking responses.[277] By utilizing three interconnected 1550 nm-VCSEL-neurons, the ON-type and OFF-type circuits in the retina were experimentally emulated. The master VCSEL (M-VCSEL), bipolar Cell VCSEL (BC-VCSEL), and retinal ganglion cell VCSEL (RGC-VCSEL) were employed to mimic the functions of photoreceptors, BCs (which generated graded potentials based on inputs from photoreceptors), and RGCs (which converted potentials into spike patterns) in the eye, respectively.

Further, an integrated all-optical neuron based on an InAs/InGaAs semiconductor laser[281] was demonstrated, capable of achieving both excitatory and inhibitory artificial neurons by adjusting the reverse voltage of the built-in saturable absorber. When the laser was biased to a single excited state emission, the excitatory neuron was activated. On the other hand, inhibitory neurons operated at the same current as the excitatory one, with the laser biased to a single ground state emission.

Table 2 presents a comparison of optoelectronic neurons in terms of device structure, neuronal function, fire frequency, and energy consumption. Research on optoelectronic neurons remains in its early stages, typically focusing on modulating neuron fire frequency through light illumination. Further exploration should extend to complex functions, such as signal transmission, lateral suppression, and frequency adaptation. The blending TS devices and photosensitive components enable optoelectronic neurons to effectively perceive and process external light signals. Semiconductor laser neurons offer considerable advantages in operating speed and firing frequency; however, challenges in integration due to their intricate optical and electrical components persist. Despite the widespread study of optoelectronic neurons, complete neural networks based on these neurons have not yet been implemented.

4. Conclusion and Outlook

Artificial neurons and synapses are crucial components for building a neuromorphic chip. Currently, research on neuromorphic devices primarily focuses on electronically controlled synapses and neurons. Emerging optoelectronic neuromorphic devices, which combine photonics, electronics, and biology, offer numerous advantages, such as reduced power consumption and expanded application fields. Utilizing optoelectronic neuromorphic devices, artificial vision systems[73,157,160,236,270] and neuromorphic computing[121,127,158,261] have been developed. Despite progress in these areas, the field remains in its early stages, facing significant challenges related to materials fabrication, array construction, and complex function realization (**Figure** 9).

4.1. Material Preparation

Photosensitive materials used in optoelectronic neuromorphic devices primarily consist of oxide semiconductors, perovskite materials, and low-dimensional materials. The bandgaps of these materials, along with their optical response wavelengths are summarized in **Table** 3. Oxide semiconductors are widely employed due to their excellent thermal and chemical stability and compatibility with CMOS processes. However, most oxide semiconductors exhibit wide bandgaps (>3.0 eV), limiting their responsiveness primarily to UV light. Although the photoionization

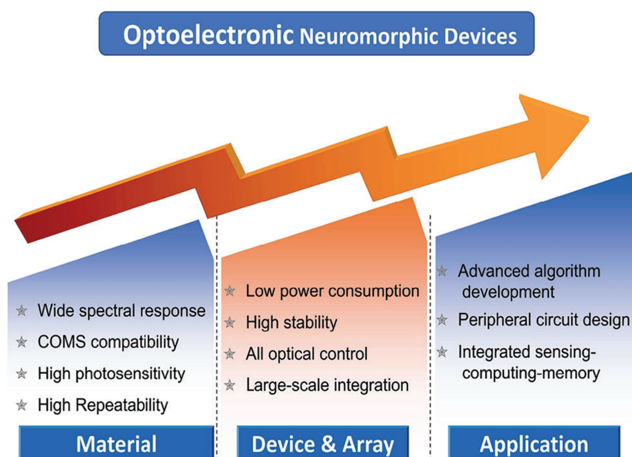

Figure 9. Overview of challenges in emerging optoelectronic neuromorphic devices.

 © 2024 The Author(s). Advanced Electronic Materials published by Wiley-VCH GmbH

Table 3. Comparison of photosensitive materials for optoelectronic neuromorphic devices.

Material type	Material	Bandgap [eV]	Operating wavelength [nm]	Ref.
Oxide	ZnO	3.2	350–800	[158]
	Zn_2SnO_4	3.88	405/633	[161]
	Ga_2O_3	4.9	255/370	[244]
	TiO_2	3.2	365/532	[96]
	IGZO	3.7	350–1000	[89]
	InZnO	3.1–3.5	275–405	[183]
	In_2O_3	3.76	360–630	[185]
	NiO	3.6	320/480	[163]
	MoO_x	3.08	350/570	[162]
2D material	WSe_2	1.2–1.6	473–655	[189]
	PbS	0.42	1940	[214]
	MoS_2	1.8	450–625	[169]
	In_2Se_3	1.4–1.6	655	[170]
	BP	0.3–2.3	280/365	[216]
Perovskite	$CsPbBr_3$	2.3	430–440	[93]
	$CH_3NH_3PbBr_3$	2.2	450–630	[198]
	$Cs_2AgBiBr_6$	2	445	[128]
	$CsPbCl_3$	2.86	365/665	[131]

of V_Os in oxides can broaden the light response wavelength to 1000 nm,[89] non-intrinsic photo-absorption severely restricts the device's photoresponsivity to long-wavelength light. This limitation hampers potential applications in artificial vision systems, underscoring the need to develop new oxide semiconductors with narrow bandgaps. In addition, combining oxides with narrow bandgap materials has been shown to effectively broaden the response wavelength range of optoelectronic devices. For example, Kang et al. demonstrated an optoelectronic synapse with broadband responses (405–830 nm) by combining IGZO, with a bandgap of 3.5 eV, and Ag_2O, with a bandgap of 1.4 eV.[210] Further, remarkable photosensitive materials with a wider responsive wavelength range (280–1940 nm), such as perovskite and low-dimensional materials, have been utilized in neuromorphic devices. However, ensuring the stability and repeatability of these devices remains a challenge due to the immature fabrication techniques of the materials used, hindering the large-scale integration of neuromorphic devices.

4.2. Device Fabrication

Optoelectronic synapses are categorized into two-terminal devices, such as memristors, and three-terminal devices, such as transistors. While the former features a simple structure and high integration density, the latter allows for effective tuning of photoelectric behaviors, including photoconductance retention characteristics and photocurrent polarities, through gate voltage. Yet, this increases the complexity of device integration and energy consumption. In recent years, attention has shifted to emerging AOC synapses, which utilize light to reversibly tune conductance, minimizing the impact of electrical signals on device stability and enriching functionality in visual simulations. However, challenges remain in this new technology. The PPC response is easily achieved due to the inherent photoelectric effect of semiconductors, while achieving a negative PPC response is much more difficult. This necessitates the design of specific device structures, such as oxide homojunctions, metal/oxide Schottky junctions, and oxide heterojunctions. Further, the working mechanisms of AOC devices often stem from the capture and release of electrons at defect states, rendering AOC behaviors highly sensitive to the types, quantities, and distribution of defects within the material. Consequently, precise control over defect states in photosensitive materials is crucial. Research on AOC devices is still in its early stages, presenting considerable opportunities for exploring their working mechanisms, device integration, and functional applications.

Research on optoelectronic neurons is relatively limited compared to optoelectronic synapses, with current efforts mainly focused on TS memristors and semiconductor lasers. TS memristors can effectively simulate neuron emission behavior through their volatile conductance switching characteristics, making them promising candidates for constructing artificial neurons. However, the operational mechanism of TS memristors typically involves the formation and rupture of conductive filaments within the device, leading to highly unpredictable performance, which impacts practical applications in neuromorphic systems. Therefore, enhancing device stability is an important future direction. Semiconductor lasers, with their high-speed operation and a wide range of neuron-like dynamics, are well-suited for laser neurons. However, implementing neuronal functions necessitates the integration of various optical and optoelectronic components, presenting considerable challenges for large-scale and high-density integration. Consequently, miniaturizing optical components is a critical development direction in this field.

4.3. Array Construction

In recent years, significant progress has been made in the development of individual optoelectronic synapses and neurons, primarily focusing on simple function simulations. However, the development of neural network hardware consisting of multiple optoelectronic neuromorphic devices is rarely reported, and current efforts fall short of building neuromorphic chips. Several key obstacles hinder the construction of large-scale neuromorphic device arrays that could mimic the complex functions of the human brain. First, device stability is insufficient for large-scale integration due to unclear working mechanisms and immature preparation processes. Second, the power consumption of optoelectronic neuromorphic devices typically falls in the microjoule range, which is significantly higher than that of biological synapses and neurons. Third, the operation of both electrical and optical signals to drive neuromorphic devices is complex. Although AOC devices have been proposed, further research is required to explore emerging techniques. Lastly, each synaptic device usually requires an independent light source to precisely control its conductance, especially during the training process of neural networks. This presents a significant challenge for integrating these light sources into each device in an array.

© 2024 The Author(s). Advanced Electronic Materials published by Wiley-VCH GmbH

2199160x, 2025, 3, Downloaded from https://advanced.onlinelibrary.wiley.com/doi/10.1002/aelm.202400482 by HONG KONG POLYTECHNIC UNIVERSITY HU NG HOM, Wiley Online Library on [24/02/2026]. See the Terms and Conditions (https://onlinelibrary.wiley.com/terms-and-conditions) on Wiley Online Library for rules of use; OA articles are governed by the applicable Creative Commons License

4.4. Complex Function Realization

One crucial application area of optoelectronic neuromorphic devices is in-sensor computing.[73,116,172,236,238,240] Inspired by the human retina, in-sensor computing has been proposed to perform part of the information processing directly within the sensor. This approach aims to reduce or eliminate data transfer and conversion at the sensor/processor interface, thereby improving the processing efficiency of visual information. Nonlinear optoelectronic responses[116] or gate-tunable positive/negative photoconductance[73,234,238,240] have been utilized for image preprocessing tasks, such as feature extraction and denoising. In addition, some optoelectronic neuromorphic devices with tunable photoresponsivity[73,172,239] have demonstrated high-level computing functionalities based on multiply-and-accumulation operations, such as image encoding and recognition. However, most complex functions, such as image recognition, still rely on software algorithms and traditional circuits. Various non-ideal factors, such as device instability and nonuniformity, may be the primary reasons limiting the complex application of devices. It is worth noting that optoelectronic neuromorphic devices can generally perform calculations in situ, meaning computations can be carried out in the memory, and they are also light-sensitive, endowing them with ISCM functions. Nevertheless, achieving ISCM function for real visual information from the external environment remains a challenge for these devices. Therefore, the development of an ISCM neuromorphic visual system is currently in progress and still has a long way to go.

In summary, research on optoelectronic devices has progressed rapidly over the past decade, integrating the characteristics of photonics, electronics and neurology. With increased collaboration among materials, devices, architectures and algorithms, it is anticipated that intricate neuromorphic functions will be realized on a chip scale in the near future.

Acknowledgements

L.H. and X.G contributed equally to this work. This research was partially supported by the National Natural Science Foundation of China (Nos. U20A20209 and 62304228), the Strategic Priority Research Program of Chinese Academy of Sciences (No. XDB32050204), the China National Postdoctoral Program for Innovative Talents (No. BX2021326), the China Postdoctoral Science Foundation (No. 2021M703310), the Zhejiang Provincial Natural Science Foundation of China (No. LQ22F040003), the Ningbo Natural Science Foundation of China (Nos. 2021J139 and 2023J356), and the Open Project of State Key Laboratory of Environment-friendly Energy Materials (No. 20kfhg09).

Conflict of Interest

The authors declare no conflict of interest.

Keywords

brain-inspired neuromorphic computing, memristors, optoelectronic neurons, optoelectronic synapses, transistors

Received: June 18, 2024
Revised: August 23, 2024
Published online: September 9, 2024

[1] S. N. Vaishnavi, A. G. Vlassenko, M. M. Rundle, A. Z. Snyder, M. A. Mintun, M. E. Raichle, *Proc. Natl. Acad. Sci. U. S. A.* **2010**, *107*, 17757.
[2] A. Sebastian, M. Le Gallo, R. Khaddam-Aljameh, E. Eleftheriou, *Nat. Nanotechnol.* **2020**, *15*, 529.
[3] Q. Xia, J. J. Yang, *Nat. Mater.* **2019**, *18*, 309.
[4] R. Pan, J. Li, F. Zhuge, L. Zhu, L. Liang, H. Zhang, J. Gao, H. Cao, B. Fu, K. Li, *Appl. Phys. Lett.* **2016**, *108*, 13504.
[5] D. Kuzum, R. G. Jeyasingh, B. Lee, H. S. Wong, *Nano Lett.* **2012**, *12*, 2179.
[6] Z. H. Tan, R. Yang, K. Terabe, X. B. Yin, X. D. Zhang, X. Guo, *Adv. Mater.* **2016**, *28*, 377.
[7] Z. Wang, T. Zeng, Y. Ren, Y. Lin, H. Xu, X. Zhao, Y. Liu, D. Ielmini, *Nat. Commun.* **2020**, *11*, 1510.
[8] L. Cai, L. Yu, W. Yue, Y. Zhu, Z. Yang, Y. Li, Y. Tao, Y. Yang, *Adv. Electron. Mater.* **2023**, *9*, 2300021.
[9] P. A. Merolla, J. V. Arthur, R. Alvarez-Icaza, A. S. Cassidy, J. Sawada, F. Akopyan, B. L. Jackson, N. Imam, C. Guo, Y. Nakamura, B. Brezzo, I. Vo, S. K. Esser, R. Appuswamy, B. Taba, A. Amir, M. D. Flickner, W. P. Risk, R. Manohar, D. S. Modha, *Science.* **2014**, *345*, 668.
[10] J. Wang, F. Zhuge, *Adv. Mater. Technol.* **2019**, *4*, 1800544.
[11] S. H. Jo, T. Chang, I. Ebong, B. B. Bhadviya, P. Mazumder, W. Lu, *Nano Lett.* **2010**, *10*, 1297.
[12] H. Zhang, B. Jiang, C. Cheng, B. Huang, H. Zhang, R. Chen, J. Xu, Y. Huang, H. Chen, W. Pei, Y. Chai, F. Zhou, *Nano Lett.* **2023**, *23*, 3107.
[13] M. Prezioso, F. Merrikh-Bayat, B. D. Hoskins, G. C. Adam, K. K. Likharev, D. B. Strukov, *Nature.* **2015**, *521*, 61.
[14] P. Yao, H. Wu, B. Gao, J. Tang, Q. Zhang, W. Zhang, J. J. Yang, H. Qian, *Nature.* **2020**, *577*, 641.
[15] S. Jung, H. Lee, S. Myung, H. Kim, S. K. Yoon, S. Kwon, Y. Ju, M. Kim, W. Yi, S. Han, B. Kwon, B. Seo, K. Lee, G. Koh, K. Lee, Y. Song, C. Choi, D. Ham, S. J. Kim, *Nature.* **2022**, *601*, 211.
[16] L. Hu, S. Fu, Y. Chen, H. Cao, L. Liang, H. Zhang, J. Gao, J. Wang, F. Zhuge, *Adv. Mater.* **2017**, *29*, 1606927.
[17] M. D. Pickett, G. Medeiros-Ribeiro, R. S. Williams, *Nat. Mater.* **2013**, *12*, 114.
[18] Q. Duan, Z. Jing, X. Zou, Y. Wang, K. Yang, T. Zhang, S. Wu, R. Huang, Y. Yang, *Nat. Commun.* **2020**, *11*, 3399.
[19] X. Zhang, W. Wang, Q. Liu, X. Zhao, J. Wei, R. Cao, Z. Yao, X. Zhu, F. Zhang, H. Lv, S. Long, M. Liu, *IEEE Electron Device Lett.* **2018**, *39*, 308.
[20] Y. Fu, Y. Zhou, X. Huang, B. Dong, F. Zhuge, Y. Li, Y. He, Y. Chai, X. Miao, *Adv. Funct. Mater.* **2022**, *32*, 2111996.
[21] L. Yan, Y. Pei, J. Wang, H. He, Y. Zhao, X. Li, Y. Wei, X. Yan, *Appl. Phys. Lett.* **2021**, *119*, 153507.
[22] X. Wang, C. Chen, L. Zhu, K. Shi, B. Peng, Y. Zhu, H. Mao, H. Long, S. Ke, C. Fu, Y. Zhu, C. Wan, Q. Wan, *Nat. Commun.* **2023**, *14*, 3444.
[23] X. Zhang, Y. Zhuo, Q. Luo, Z. Wu, R. Midya, Z. Wang, W. Song, R. Wang, N. K. Upadhyay, Y. Fang, F. Kiani, M. Rao, Y. Yang, Q. Xia, Q. Liu, M. Liu, J. J. Yang, *Nat. Commun.* **2020**, *11*, 51.
[24] H. Zhao, Z. Liu, J. Tang, B. Gao, Q. Qin, J. Li, Y. Zhou, P. Yao, Y. Xi, Y. Lin, H. Qian, H. Wu, *Nat. Commun.* **2023**, *14*, 2276.
[25] R. Wang, T. Shi, X. Zhang, J. Wei, J. Lu, J. Zhu, Z. Wu, Q. Liu, M. Liu, *Nat. Commun.* **2022**, *13*, 2289.
[26] E. J. Fuller, S. T. Keene, A. Melianas, Z. Wang, S. Agarwal, Y. Li, Y. Tuchman, C. D. James, M. J. Marinella, J. J. Yang, A. Salleo, A. A. Talin, *Science.* **2019**, *364*, 570.
[27] X. Liang, Y. Luo, Y. Pei, M. Wang, C. Liu, *Nat. Electron.* **2022**, *5*, 859.
[28] J. Cui, F. An, J. Qian, Y. Wu, L. L. Sloan, S. Pidaparthy, J. Zuo, Q. Cao, *Nat. Electron.* **2023**, *6*, 292.
[29] L. Danial, E. Pikhay, E. Herbelin, N. Wainstein, V. Gupta, N. Wald, Y. Roizin, R. Daniel, S. Kvatinsky, *Nat. Electron.* **2019**, *2*, 596.

© 2024 The Author(s). Advanced Electronic Materials published by Wiley-VCH GmbH

2199160x, 2025, 3, Downloaded from https://advanced.onlinelibrary.wiley.com/doi/10.1002/aelm.202400482 by HONG KONG POLYTECHNIC UNIVERSITY HU NG HOM, Wiley Online Library on [24/02/2026]. See the Terms and Conditions (https://onlinelibrary.wiley.com/terms-and-conditions) on Wiley Online Library for rules of use; OA articles are governed by the applicable Creative Commons License

[30] C. Pan, C. Wang, S. Liang, Y. Wang, T. Cao, P. Wang, C. Wang, S. Wang, B. Cheng, A. Gao, E. Liu, K. Watanabe, T. Taniguchi, F. Miao, *Nat. Electron.* **2020**, *3*, 383.
[31] Y. van de Burgt, E. Lubberman, E. J. Fuller, S. T. Keene, G. C. Faria, S. Agarwal, M. J. Marinella, T. A. Alec, A. Salleo, *Nat. Mater.* **2017**, *16*, 414.
[32] J. Han, M. Seo, J. Yu, Y. Suh, Y. Choi, *IEEE Electron Device Lett.* **2020**, *41*, 1157.
[33] C. Ge, C. X. Liu, Q. L. Zhou, Q. H. Zhang, J. Y. Du, J. K. Li, C. Wang, L. Gu, G. Z. Yang, K. J. Jin, *Adv. Mater.* **2019**, *31*, 1900379.
[34] M. T. Sharbati, Y. Du, J. Torres, N. D. Ardolino, M. Yun, F. Xiong, *Adv. Mater.* **2018**, *30*, 1802353.
[35] L. Q. Zhu, C. J. Wan, L. Q. Guo, Y. Shi, Q. Wan, *Nat. Commun.* **2014**, *5*, 3158.
[36] K. Ding, J. Wang, Y. Zhou, H. Tian, L. Lu, R. Mazzarello, C. Jia, W. Zhang, F. Rao, E. Ma, *Science.* **2019**, *366*, 210.
[37] X. Mou, J. Tang, Y. Lyu, Q. Zhang, S. Yang, F. Xu, W. Liu, M. Xu, Y. Zhou, W. Sun, Y. Zhong, B. Gao, P. Yu, H. Qian, H. Wu, *Sci. Adv.* **2021**, *7*, eabh0648.
[38] C. D. Wright, P. Hosseini, J. A. V. Diosdado, *Adv. Funct. Mater.* **2013**, *23*, 2248.
[39] A. P. M. L. Tomas Tuma, *Nat. Nanotechnol.* **2016**, *11*, 693.
[40] D. Kuzum, R. G. D. Jeyasingh, B. Lee, H. S. P. Wong, *Nano Lett.* **2012**, *12*, 2179.
[41] Y. Li, Y. Zhong, J. Zhang, L. Xu, Q. Wang, H. Sun, H. Tong, X. Cheng, X. Miao, *Sci. Rep.* **2014**, *4*, 4906.
[42] D. H. Lim, S. Wu, R. Zhao, J. H. Lee, H. Jeong, L. Shi, *Nat. Commun.* **2021**, *12*, 319.
[43] O. Bichler, M. Suri, D. Querlioz, D. Vuillaume, B. Desalvo, C. Gamrat, *IEEE Trans. Electron Devices.* **2012**, *59*, 2206.
[44] P. Krzysteczko, J. Münchenberger, M. Schäfers, G. Reiss, A. Thomas, *Adv. Mater.* **2012**, *24*, 762.
[45] A. H. Lone, H. Fariborzi, *IEEE Trans. Electron Devices.* **2023**, *70*, 371.
[46] A. Kurenkov, S. Duttagupta, C. Zhang, S. Fukami, Y. Horio, H. Ohno, *Adv. Mater.* **2019**, *31*, 1900636.
[47] K. M. Song, J. Jeong, B. Pan, X. Zhang, J. Xia, S. Cha, T. Park, K. Kim, S. Finizio, J. Raabe, J. Chang, Y. Zhou, W. Zhao, W. Kang, H. Ju, S. Woo, *Nat. Electron.* **2020**, *3*, 148.
[48] W. Hu, Z. Zhang, Y. Liao, Q. Li, Y. Shi, H. Zhang, X. Zhang, C. Niu, Y. Wu, W. Yu, X. Zhou, H. Guo, W. Wang, J. Xiao, L. Yin, Q. Liu, J. Shen, *Nat. Commun.* **2023**, *14*, 2562.
[49] Y. Cao, A. Rushforth, Y. Sheng, H. Zheng, K. Wang, *Adv. Funct. Mater.* **2019**, *29*, 1808104.
[50] J. Torrejon, M. Riou, F. A. Araujo, S. Tsunegi, G. Khalsa, D. Querlioz, P. Bortolotti, V. Cros, K. Yakushiji, A. Fukushima, H. Kubota, S. Yuasa, M. D. Stiles, J. Grollier, *Nature* **2017**, *547*, 428.
[51] D. Kim, Y. Jeon, B. Ku, C. Chung, T. H. Kim, S. Yang, U. Won, T. Jeong, C. Choi, *ACS Appl. Mater. Interfaces.* **2021**, *13*, 52743.
[52] Y. Peng, N. Xu, T. K. Liu, Y. Hao, W. Xiao, G. Han, Y. Liu, J. Wu, K. Wang, Y. He, Z. Yu, X. Wang, *IEEE Electron Device Lett.* **2019**, *40*, 1933.
[53] Z. Luo, S. Zhang, Y. Liu, D. Zhang, X. Gan, J. Seidel, Y. Liu, G. Han, M. Alexe, Y. Hao, *ACS Nano.* **2022**, *16*, 3362.
[54] M. Yan, Q. Zhu, S. Wang, Y. Ren, G. Feng, L. Liu, H. Peng, Y. He, J. Wang, P. Zhou, X. Meng, X. Tang, J. Chu, B. Dkhil, B. Tian, C. Duan, *Adv. Electron. Mater.* **2021**, *7*, 2001276.
[55] Z. Dang, F. Guo, H. Duan, Q. Zhao, Y. Fu, W. Jie, K. Jin, J. Hao, *Nano Lett.* **2023**, *23*, 6752.
[56] C. Gastaldi, S. Kamaei, M. Cavalieri, A. Saeidi, I. Stolichnov, I. Radu, A. M. Ionescu, *IEEE Electron Device Lett.* **2023**, *44*, 678.
[57] M. K. Kim, I. J. Kim, J. S. Lee, *Sci. Adv.* **2022**, *8*, eabm8537.
[58] J. Q. Yang, R. Wang, Y. Ren, J. Y. Mao, Z. P. Wang, Y. Zhou, S. T. Han, *Adv. Mater.* **2020**, *32*, 2003610.
[59] K. He, C. Wang, Y. He, J. Su, X. Chen, *Chem. Rev.* **2023**, *123*, 13796.
[60] S. Choi, J. Yang, G. Wang, *Adv. Mater.* **2020**, *32*, 2004659.
[61] Y. Zhang, Z. Wang, J. Zhu, Y. Yang, M. Rao, W. Song, Y. Zhuo, X. Zhang, M. Cui, L. Shen, R. Huang, J. J. Yang, *Appl. Phys. Rev.* **2020**, *7*, 11308.
[62] D. Kuzum, S. Yu, H. P. Wong, *Nanotechnology.* **2013**, *24*, 382001.
[63] A. F. Benner, M. Ignatowski, J. A. Kash, D. M. Kuchta, M. B. Ritter, *IBM J. Res. Dev.* **2005**, *49*, 755.
[64] B. J. Shastri, A. N. Tait, T. Ferreira De Lima, W. H. P. Pernice, H. Bhaskaran, C. D. Wright, P. R. Prucnal, *Nat. Photonics.* **2021**, *15*, 102.
[65] M. Lee, H. Seung, J. I. Kwon, M. K. Choi, D. Kim, C. Choi, *ACS Omega.* **2023**, *8*, 5209.
[66] X. Wang, Y. Zong, D. Liu, J. Yang, Z. Wei, *Adv. Funct. Mater.* **2023**, *33*, 2213894.
[67] W. Wang, S. Gao, Y. Wang, Y. Li, W. Yue, H. Niu, F. Yin, Y. Guo, G. Shen, *Adv. Sci.* **2022**, *9*, 2105577.
[68] Y. Sun, Y. Ding, D. Xie, *Adv. Funct. Mater.* **2021**, *31*, 2105625.
[69] Y. Wu, W. Deng, X. Wang, W. Yu, Z. Chen, X. Chen, J. Li, Y. Chai, Y. Zhang, *Adv. Funct. Mater.* **2023**, *33*, 2302899.
[70] J. Y. Mao, L. Zhou, X. Zhu, Y. Zhou, S. T. Han, *Adv. Opt. Mater.* **2019**, *7*, 1900766.
[71] X. Han, Z. Xu, W. Wu, X. Liu, P. Yan, C. Pan, *Small Struct.* **2020**, *1*, 2000029.
[72] S. Seo, S. H. Jo, S. Kim, J. Shim, S. Oh, J. H. Kim, K. Heo, J. W. Choi, C. Choi, S. Oh, D. Kuzum, H. P. Wong, J. H. Park, *Nat. Commun.* **2018**, *9*, 5106.
[73] L. Mennel, J. Symonowicz, S. Wachter, D. K. Polyushkin, A. J. Molina-Mendoza, T. Mueller, *Nature.* **2020**, *579*, 62.
[74] T. Dresbach, B. Qualmann, M. M. Kessels, C. C. Garner, E. D. Gundelfinger, *Cell. Mol. Life Sci.* **2001**, *58*, 94.
[75] C. N. Liu, M. Michaelis, R. Amir, M. Devor, *J. Neurophysiol.* **2000**, *84*, 205.
[76] L. M. Palmer, G. J. Stuart, *J. Neurosci.* **2009**, *29*, 6897.
[77] M. Kumar, H. S. Kim, J. Kim, *Adv. Mater.* **2019**, *31*, 1900021.
[78] Q. Wu, B. Dang, C. Lu, G. Xu, G. Yang, J. Wang, X. Chuai, N. Lu, D. Geng, H. Wang, L. Li, *Nano Lett.* **2020**, *20*, 8015.
[79] H. Yonezu, A. Miho, T. Himeno, K. Pak, Y. Takano, *Electron. Lett.* **1989**, *25*, 670.
[80] J. M. Shainline, S. M. Buckley, A. N. Mccaughan, J. Chiles, A. Jafari-Salim, R. P. Mirin, S. W. Nam, *J. Appl. Phys.* **2018**, *124*, 152130.
[81] M. A. Mishchenko, S. A. Gerasimova, A. V. Lebedeva, L. S. Lepekhina, A. N. Pisarchik, V. B. Kazantsev, *PLoS One.* **2018**, *13*, 0198396.
[82] Y. Dan, Z. Fan, Q. Chen, Y. Lai, X. Sun, T. Zhang, K. Xu, *Front. Phys.* **2022**, *10*, 1064693.
[83] X. Yuan, Y. Wang, Z. Xu, T. Zhou, L. Fang, *Nat. Commun.* **2023**, *14*, 7110.
[84] T. J. Lee, K. R. Yun, S. K. Kim, J. H. Kim, J. Jin, K. B. Sim, D. H. Lee, G. W. Hwang, T. Y. Seong, *Adv. Mater.* **2021**, *33*, 2105485.
[85] J. Han, D. Geum, M. Lee, J. Yu, S. K. Kim, S. Kim, Y. Choi, *Nano Lett.* **2020**, *20*, 8781.
[86] M. Mayford, S. A. Siegelbaum, E. R. Kandel, *Cold Spring Harbor Perspect. Biol.* **2012**, *4*, a005751.
[87] M. H. Hennig, *Front. Comput. Neurosci.* **2013**, *7*, 45.
[88] L. Hu, J. Yang, J. Wang, P. Cheng, L. O. Chua, F. Zhuge, *Arxiv:2004.08077* **2020**, https://doi.org/10.48550/arXiv.2004.08077.
[89] L. Hu, J. Yang, J. Wang, P. Cheng, L. O. Chua, F. Zhuge, *Adv. Funct. Mater.* **2021**, *31*, 2005582.
[90] D. Hu, R. Yang, L. Jiang, X. Guo, *ACS Appl. Mater. Interfaces.* **2018**, *10*, 6463.
[91] H. K. He, R. Yang, W. Zhou, H. M. Huang, J. Xiong, L. Gan, T. Y. Zhai, X. Guo, *Small.* **2018**, *14*, 1800079.
[92] J. J. Yu, L. Y. Liang, L. X. Hu, H. X. Duan, W. H. Wu, H. L. Zhang, J. H. Gao, F. Zhuge, T. C. Chang, H. T. Cao, *Nano Energy.* **2019**, *62*, 772.

 © 2024 The Author(s). Advanced Electronic Materials published by Wiley-VCH GmbH

2199160x, 2025, 3, Downloaded from https://advanced.onlinelibrary.wiley.com/doi/10.1002/aelm.202400482 by HONG KONG POLYTECHNIC UNIVERSITY HU NG HOM, Wiley Online Library on [24/02/2026]. See the Terms and Conditions (https://onlinelibrary.wiley.com/terms-and-conditions) on Wiley Online Library for rules of use; OA articles are governed by the applicable Creative Commons License

[93] B. Pradhan, S. Das, J. Li, F. Chowdhury, J. Cherusseri, D. Pandey, D. Dev, A. Krishnaprasad, E. Barrios, A. Towers, A. Gesquiere, L. Tetard, T. Roy, J. Thomas, *Sci. Adv.* **2020**, *6*, eaay5225.
[94] X. Zhu, W. D. Lu, *ACS Nano.* **2018**, *12*, 1242.
[95] G. Agnus, W. Zhao, V. Derycke, A. Filoramo, Y. Lhuillier, S. Lenfant, D. Vuillaume, C. Gamrat, J. P. Bourgoin, *Adv. Mater.* **2010**, *22*, 702.
[96] X. Shan, C. Zhao, X. Wang, Z. Wang, S. Fu, Y. Lin, T. Zeng, X. Zhao, H. Xu, X. Zhang, Y. Liu, *Adv. Sci.* **2022**, *9*, 2104632.
[97] S. Shrivastava, H. Chi, S. E. Limantoro, H. Juliano, T. Tseng, *Appl. Phys. Lett.* **2024**, *124*, 133503.
[98] M. Karbalaei Akbari, R. K. Ramachandran, C. Detavernier, J. Hu, J. Kim, F. Verpoort, S. Zhuiykov, *J. Mater. Chem. C.* **2021**, *9*, 2539.
[99] D. Kumar, S. Shrivastava, A. Saleem, A. Singh, H. Lee, Y. Wang, T. Tseng, *ACS Appl. Electron. Mater.* **2022**, *4*, 2180.
[100] J. Lao, W. Xu, C. Jiang, N. Zhong, B. Tian, H. Lin, C. Luo, J. Travas Sejdic, H. Peng, C. G. Duan, *Adv. Electron. Mater.* **2021**, *7*, 2100291.
[101] M. Kumar, S. Abbas, J. Kim, *ACS Appl. Mater. Interfaces.* **2018**, *10*, 34370.
[102] L. Chua, *IEEE Trans. Circuits Syst.* **1971**, *18*, 507.
[103] D. B. Strukov, G. S. Snider, D. R. Stewart, R. S. Williams, *Nature.* **2008**, *453*, 80.
[104] A. Serb, J. Bill, A. Khiat, R. Berdan, R. Legenstein, T. Prodromakis, *Nat. Commun.* **2016**, *7*, 12611.
[105] T. Fu, X. Liu, H. Gao, J. E. Ward, X. Liu, B. Yin, Z. Wang, Y. Zhuo, D. Walker, Y. J. Joshua, J. Chen, D. R. Lovley, J. Yao, *Nat. Commun.* **2020**, *11*, 1861.
[106] P. Liu, F. Hui, F. Aguirre, F. Saiz, L. Tian, T. Han, Z. Zhang, E. Miranda, M. Lanza, *Adv. Mater.* **2022**, *34*, 2201197.
[107] I. Boybat, M. Le Gallo, S. R. Nandakumar, T. Moraitis, T. Parnell, T. Tuma, B. Rajendran, Y. Leblebici, A. Sebastian, E. Eleftheriou, *Nat. Commun.* **2018**, *9*, 2514.
[108] C. J. O'Kelly, J. A. Fairfield, D. Mccloskey, H. G. Manning, J. F. Donegan, J. J. Boland, *Adv. Electron. Mater.* **2016**, *2*, 1500458.
[109] S. Jeon, S. Ahn, I. Song, C. J. Kim, U. Chung, E. Lee, I. Yoo, A. Nathan, S. Lee, K. Ghaffarzadeh, J. Robertson, K. Kim, *Nat. Mater.* **2012**, *11*, 301.
[110] W. Zhou, R. Yang, H. He, H. Huang, J. Xiong, X. Guo, *Appl. Phys. Lett.* **2018**, *113*, 61107.
[111] B. Zhao, M. Xiao, D. Shen, Y. N. Zhou, *Nanotechnology.* **2020**, *31*, 125201.
[112] H. Tan, Q. Tao, I. Pande, S. Majumdar, F. Liu, Y. Zhou, P. Persson, J. Rosen, S. van Dijken, *Nat. Commun.* **2020**, *11*, 1369.
[113] Y. Zhu, C. Wu, Z. Xu, Y. Liu, H. Hu, T. Guo, T. W. Kim, Y. Chai, F. Li, *Nano Lett.* **2021**, *21*, 6087.
[114] Z. Zhou, Y. Pei, J. Zhao, G. Fu, X. Yan, *Appl. Phys. Lett.* **2021**, *118*, 191103.
[115] X. Shan, C. Zhao, Y. Lin, J. Liu, X. Zhang, Y. Tao, C. Wang, X. Zhao, Z. Wang, H. Xu, Y. Liu, *Appl. Phys. Lett.* **2022**, *121*, 26350.
[116] F. Zhou, Z. Zhou, J. Chen, T. H. Choy, J. Wang, N. Zhang, Z. Lin, S. Yu, J. Kang, H. P. Wong, Y. Chai, *Nat. Nanotechnol.* **2019**, *14*, 776.
[117] H. Tan, G. Liu, H. Yang, X. Yi, L. Pan, J. Shang, S. Long, M. Liu, Y. Wu, R. Li, *ACS Nano.* **2017**, *11*, 11298.
[118] S. Gao, G. Liu, H. Yang, C. Hu, Q. Chen, G. Gong, W. Xue, X. Yi, J. Shang, R. W. Li, *ACS Nano.* **2019**, *13*, 2634.
[119] Y. Fang, Q. Li, J. Meng, T. Wang, H. Zhu, Q. Q. Sun, D. W. Zhang, L. Chen, *Adv. Electron. Mater.* **2023**, *9*, 2300120.
[120] Y. Q. Hu, W. Xu, N. T. Liu, Y. K. Li, X. Deng, Z. Guan, Y. F. Zheng, S. Yang, R. Huang, F. Y. Yue, Y. Y. Zhang, H. Peng, B. B. Chen, N. Zhong, P. H. Xiang, C. G. Duan, *Adv. Opt. Mater.* **2024**, *12*, 2302887.
[121] Y. Sun, Q. Li, X. Zhu, C. Liao, Y. Wang, Z. Li, S. Liu, H. Xu, W. Wang, *Adv. Intell. Syst.* **2023**, *5*, 2200196.
[122] A. Mehonic, T. Gerard, A. J. Kenyon, *Appl. Phys. Lett.* **2017**, *111*, 233502.
[123] Y. Chen, Q. Wei, J. Yin, Y. Xia, Z. Liu, *Adv. Electron. Mater.* **2018**, *4*, 1800242.
[124] K. Zhang, D. Meng, F. Bai, J. Zhai, Z. L. Wang, *Adv. Funct. Mater.* **2020**, *30*, 2002945.
[125] Y. Pei, L. Yan, Z. Wu, J. Lu, J. Zhao, J. Chen, Q. Liu, X. Yan, *ACS Nano.* **2021**, *15*, 17319.
[126] W. Wang, S. Gao, Y. Li, W. Yue, H. Kan, C. Zhang, Z. Lou, L. Wang, G. Shen, *Adv. Funct. Mater.* **2021**, *31*, 2101201.
[127] L. Sun, Z. Wang, J. Jiang, Y. Kim, B. Joo, S. Zheng, S. Lee, W. J. Yu, B. S. Kong, H. Yang, *Sci. Adv.* **2021**, *7*, eabg1455.
[128] J. Lao, M. Yan, B. Tian, C. Jiang, C. Luo, Z. Xie, Q. Zhu, Z. Bao, N. Zhong, X. Tang, L. Sun, G. Wu, J. Wang, H. Peng, J. Chu, C. Duan, *Adv. Sci.* **2022**, *9*, 2106092.
[129] X. Guan, W. Hu, M. A. Haque, N. Wei, Z. Liu, A. Chen, T. Wu, *Adv. Funct. Mater.* **2018**, *28*, 1704665.
[130] F. Ma, Y. Zhu, Z. Xu, Y. Liu, X. Zheng, S. Ju, Q. Li, Z. Ni, H. Hu, Y. Chai, C. Wu, T. W. Kim, F. Li, *Adv. Funct. Mater.* **2020**, *30*, 1908901.
[131] L. Yang, M. Singh, S. W. Shen, K. Y. Chih, S. W. Liu, C. I. Wu, C. W. Chu, H. W. Lin, *Adv. Funct. Mater.* **2021**, *31*, 2008259.
[132] R. Waser, R. Dittmann, G. Staikov, K. Szot, *Adv. Mater.* **2009**, *21*, 2632.
[133] X. Zhao, J. Niu, Y. Yang, X. Xiao, R. Chen, Z. Wu, Y. Zhang, H. Lv, S. Long, Q. Liu, C. Jiang, M. Liu, *Nanotechnology.* **2020**, *31*, 144002.
[134] Z. Wang, S. Joshi, S. E. Savel'Ev, H. Jiang, R. Midya, P. Lin, M. Hu, N. Ge, J. P. Strachan, Z. Li, Q. Wu, M. Barnell, G. Li, H. L. Xin, R. S. Williams, Q. Xia, J. J. Yang, *Nat. Mater.* **2017**, *16*, 101.
[135] F. Zhuge, K. Li, B. Fu, H. Zhang, J. Li, H. Chen, L. Liang, J. Gao, H. Cao, Z. Liu, H. Luo, *AIP Adv.* **2015**, *5*, 57125.
[136] Y. Wang, J. Yang, Z. Wang, J. Chen, Q. Yang, Z. Lv, Y. Zhou, Y. Zhai, Z. Li, S. T. Han, *Small.* **2019**, *15*, 1805431.
[137] Y. Zhou, K. S. Yew, D. S. Ang, T. Kawashima, M. K. Bera, H. Z. Zhang, G. Bersuker, *Appl. Phys. Lett.* **2015**, *107*, 72107.
[138] N. Yang, C. Hu, Z. Ren, S. Bao, B. Tian, F. Yue, P. Xiang, N. Zhong, C. Duan, J. Chu, *ACS Appl. Electron. Mater.* **2020**, *2*, 1035.
[139] C. F. Huebner, V. Tsyalkovsky, Y. Bandera, M. K. Burdette, J. A. Shetzline, C. Tonkin, S. E. Creager, S. H. Foulger, *Nanoscale.* **2015**, *7*, 1270.
[140] F. Zhou, Y. Liu, X. Shen, M. Wang, F. Yuan, Y. Chai, *Adv. Funct. Mater.* **2018**, *28*, 1800080.
[141] X. Zhao, Z. Wang, W. Li, S. Sun, H. Xu, P. Zhou, J. Xu, Y. Lin, Y. Liu, *Adv. Funct. Mater.* **2020**, *30*, 1910151.
[142] Y. Wang, S. Chen, X. Cheng, W. Chen, Z. Xiong, Z. Lv, C. Wu, L. Wang, G. Zhang, X. Zhu, L. Luo, S. T. Han, *Adv. Funct. Mater.* **2024**, *34*, 2309807.
[143] S. Sharma, A. Kumar, S. Dutta, D. Kaur, *Appl. Phys. Lett.* **2020**, *117*, 192101.
[144] X. Fu, T. Li, B. Cai, J. Miao, G. N. Panin, X. Ma, J. Wang, X. Jiang, Q. Li, Y. Dong, C. Hao, J. Sun, H. Xu, Q. Zhao, M. Xia, B. Song, F. Chen, X. Chen, W. Lu, W. Hu, *Light: Sci. Appl.* **2023**, *12*, 39.
[145] S. Ham, S. Choi, H. Cho, S. I. Na, G. Wang, *Adv. Funct. Mater.* **2019**, *29*, 1806646.
[146] Y. Zhou, D. Liu, J. Wang, Z. Cheng, L. Liu, N. Yang, Y. Liu, T. Xia, X. Liu, X. Zhang, C. Ye, Z. Xu, W. Xiong, P. K. Chu, X. Yu, *ACS Appl. Mater. Interfaces.* **2020**, *12*, 25108.
[147] A. H. Jaafar, M. O'Neill, S. M. Kelly, E. Verrelli, N. T. Kemp, *Adv. Electron. Mater.* **2019**, *5*, 1900197.
[148] Z. Xie, K. Jiang, S. Zhang, J. Ben, M. Liu, S. Lv, Y. Chen, Y. Jia, X. Sun, D. Li, *Light: Sci. Appl.* **2024**, *13*, 78.
[149] P. Maier, F. Hartmann, M. R. Sousa Dias, M. Emmerling, C. Schneider, L. K. Castelano, M. Kamp, G. E. Marques, V. Lopez-Richard, L. Worschech, S. Höfling, *Appl. Phys. Lett.* **2016**, *109*, 23501.
[150] H. R. El, V. Humbert, V. Rouco, G. Sanchez-Santolino, A. Lagarrigue, K. Seurre, S. J. Carreira, A. Sander, J. Charliac, S. Mesoraca, J.

© 2024 The Author(s). Advanced Electronic Materials published by Wiley-VCH GmbH

2199160x, 2025, 3, Downloaded from https://advanced.onlinelibrary.wiley.com/doi/10.1002/aelm.202400482 by HONG KONG POLYTECHNIC UNIVERSITY HU NG HOM, Wiley Online Library on [24/02/2026]. See the Terms and Conditions (https://onlinelibrary.wiley.com/terms-and-conditions) on Wiley Online Library for rules of use; OA articles are governed by the applicable Creative Commons License

Trastoy, J. Briatico, J. Santamaria, J. E. Villegas, *Nat. Commun.* **2023**, *14*, 3010.
[151] P. Maier, F. Hartmann, M. Emmerling, C. Schneider, M. Kamp, S. Höfling, L. Worschech, *Phys. Rev. Appl.* **2016**, *5*, 54011.
[152] V. A. Volodin, G. N. Kamaev, M. Vergnat, *Phys. Status Solidi RRL.* **2020**, *14*, 2000165.
[153] J. Zhu, T. Zhang, Y. Yang, R. Huang, *Appl. Phys. Rev.* **2020**, *7*, 11312.
[154] K. Liao, P. Lei, M. Tu, S. Luo, T. Jiang, W. Jie, J. Hao, *ACS Appl. Mater. Interfaces.* **2021**, *13*, 32606.
[155] X. Zhuge, J. Wang, F. Zhuge, *Phys. Status Solidi RRL.* **2019**, *13*, 1900082.
[156] X. Pan, T. Jin, J. Gao, C. Han, Y. Shi, W. Chen, *Small.* **2020**, *16*, 2001504.
[157] L. Hu, J. Shao, J. Wang, P. Cheng, L. Zhang, Y. Chai, Z. Ye, F. Zhuge, *Appl. Phys. Rev.* **2024**, *11*, 11411.
[158] J. Yang, L. Hu, L. Shen, J. Wang, P. Cheng, H. Lu, F. Zhuge, Z. Ye, *Fundam. Res.* **2024**, *4*, 158.
[159] B. Cai, Y. Huang, L. Tang, T. Wang, C. Wang, Q. Sun, D. W. Zhang, L. Chen, *Adv. Funct. Mater.* **2023**, *33*, 2306272.
[160] G. Zhou, J. Li, Q. Song, L. Wang, Z. Ren, B. Sun, X. Hu, W. Wang, G. Xu, X. Chen, L. Cheng, F. Zhou, S. Duan, *Nat. Commun.* **2023**, *14*, 8489.
[161] S. Shrivastava, L. B. Keong, S. Pratik, A. S. Lin, T. Y. Tseng, *Adv. Electron. Mater.* **2023**, *9*, 2201093.
[162] J. Zheng, Y. Du, Y. Dong, X. Shan, Y. Tao, Y. Lin, X. Zhao, Z. Wang, H. Xu, Y. Liu, *Appl. Phys. Lett.* **2024**, *124*, 133502.
[163] C. Lu, J. Meng, J. Song, T. Wang, H. Zhu, Q. Sun, D. W. Zhang, L. Chen, *Nano Lett.* **2024**, *24*, 1667.
[164] Q. Sun, Z. Guo, X. Zhu, Q. Jiang, H. Liu, X. Liu, C. Sun, Y. Zhang, L. Wu, R. Li, *Nanoscale.* **2023**, *15*, 10050.
[165] Y. Fu, H. Dai, J. Li, C. Wang, D. Zhao, X. Zhang, C. Liu, Q. Lu, Y. Wang, Y. Xiao, S. Feng, *ACS Photonics.* **2024**, *11*, 1548.
[166] Y. Chang, J. Jian, *Carbon.* **2023**, *202*, 167.
[167] C. Diorio, P. Hasler, A. Minch, C. A. Mead, *IEEE Trans. Electron Devices.* **1996**, *43*, 1972.
[168] M. Lee, W. Lee, S. Choi, J. W. Jo, J. Kim, S. K. Park, Y. H. Kim, *Adv. Mater.* **2017**, *29*, 1700951.
[169] A. Dodda, D. Jayachandran, A. Pannone, N. Trainor, S. P. Stepanoff, M. A. Steves, S. S. Radhakrishnan, S. Bachu, C. W. Ordonez, J. R. Shallenberger, J. M. Redwing, K. L. Knappenberger, D. E. Wolfe, S. Das, *Nat. Mater.* **2022**, *21*, 1379.
[170] K. Liu, T. Zhang, B. Dang, L. Bao, L. Xu, C. Cheng, Z. Yang, R. Huang, Y. Yang, *Nat. Electron.* **2022**, *5*, 761.
[171] Y. Zhou, J. Fu, Z. Chen, F. Zhuge, Y. Wang, J. Yan, S. Ma, L. Xu, H. Yuan, M. Chan, X. Miao, Y. He, Y. Chai, *Nat. Electron.* **2023**, *6*, 870.
[172] G. Wu, X. Zhang, G. Feng, J. Wang, K. Zhou, J. Zeng, D. Dong, F. Zhu, C. Yang, X. Zhao, D. Gong, M. Zhang, B. Tian, C. Duan, Q. Liu, J. Wang, J. Chu, M. Liu, *Nat. Mater.* **2023**, *22*, 1499.
[173] P. Y. Huang, B. Y. Jiang, H. J. Chen, J. Y. Xu, K. Wang, C. Y. Zhu, X. Y. Hu, D. Li, L. Zhen, F. C. Zhou, J. K. Qin, C. Y. Xu, *Nat. Commun.* **2023**, *14*, 6736.
[174] A. Dodda, N. Trainor, J. M. Redwing, S. Das, *Nat. Commun.* **2022**, *13*, 3587.
[175] Q. Wu, J. Wang, J. Cao, C. Lu, G. Yang, X. Shi, X. Chuai, Y. Gong, Y. Su, Y. Zhao, N. Lu, D. Geng, H. Wang, L. Li, M. Liu, *Adv. Electron. Mater.* **2018**, *4*, 1800556.
[176] J. Kim, S. Song, J. M. Lee, S. Nam, J. Kim, D. K. Hwang, S. K. Park, Y. H. Kim, *Small.* **2023**, *19*, 2301186.
[177] T. Kim, J. W. Lim, S. J. Yun, S. H. Lee, K. H. Jung, *Adv. Electron. Mater.* **2020**, *6*, 1901044.
[178] M. C. Tai, Y. X. Wang, T. C. Chang, C. C. Lin, Y. F. Tu, Y. H. Hung, F. M. Ciou, Y. S. Lin, S. Sze, *Adv. Electron. Mater.* **2020**, *6*, 2000747.
[179] J. Sun, S. Oh, Y. Choi, S. Seo, M. J. Oh, M. Lee, W. B. Lee, P. J. Yoo, J. H. Cho, J. H. Park, *Adv. Funct. Mater.* **2018**, *28*, 1804397.
[180] W. Qiu, Y. Huang, L. A. Kong, Y. Chen, W. Liu, Z. Wang, J. Sun, Q. Wan, J. H. Cho, J. Yang, Y. Gao, *Adv. Funct. Mater.* **2020**, *30*, 2002325.
[181] M. K. Kim, J. S. Lee, *Adv. Mater.* **2020**, *32*, 1907826.
[182] S. Feng, J. Li, L. Feng, Z. Liu, J. Wang, C. Cui, O. Zhou, L. Deng, H. Xu, B. Leng, X. Q. Chen, X. Jiang, B. Liu, X. Zhang, *Adv. Mater.* **2023**, *35*, 2308090.
[183] J. Wang, Y. Chen, L. Kong, Y. Fu, Y. Gao, J. Sun, *Appl. Phys. Lett.* **2018**, *113*, 151101.
[184] H. K. Li, T. P. Chen, P. Liu, S. G. Hu, Y. Liu, Q. Zhang, P. S. Lee, *J. Appl. Phys.* **2016**, *119*, 244505.
[185] Q. Liu, L. Yin, C. Zhao, Z. Wu, J. Wang, X. Yu, Z. Wang, W. Wei, Y. Liu, I. Z. Mitrovic, L. Yang, E. G. Lim, C. Z. Zhao, *Nano Energy.* **2022**, *97*, 107171.
[186] C. Jin, W. Liu, Y. Xu, Y. Huang, Y. Nie, X. Shi, G. Zhang, P. He, J. Zhang, H. Cao, J. Sun, J. Yang, *Nano Lett.* **2022**, *22*, 3372.
[187] G. Li, D. Xie, H. Zhong, Z. Zhang, X. Fu, Q. Zhou, Q. Li, H. Ni, J. Wang, E. J. Guo, M. He, C. Wang, G. Yang, K. Jin, C. Ge, *Nat. Commun.* **2022**, *13*, 1729.
[188] N. Duan, Y. Li, H. Chiang, J. Chen, W. Pan, Y. Zhou, Y. Chien, Y. He, K. Xue, G. Liu, T. Chang, X. Miao, *Nanoscale* **2019**, *11*, 17590.
[189] X. Hou, C. Liu, Y. Ding, L. Liu, S. Wang, P. Zhou, *Adv. Sci.* **2020**, *7*, 2002072.
[190] H. Jang, C. Liu, H. Hinton, M. H. Lee, H. Kim, M. Seol, H. J. Shin, S. Park, D. Ham, *Adv. Mater.* **2020**, *32*, 2002431.
[191] S. Li, Z. Zhang, X. Chen, W. Deng, Y. Lu, M. Sui, F. Gong, G. Xu, X. Li, F. Liu, C. You, F. Chu, Y. Wu, H. Yan, Y. Zhang, *Adv. Mater.* **2022**, *34*, 2107734.
[192] C. Choi, J. Leem, M. Kim, A. Taqieddin, C. Cho, K. W. Cho, G. J. Lee, H. Seung, H. J. Bae, Y. M. Song, T. Hyeon, N. R. Aluru, S. Nam, D. Kim, *Nat. Commun.* **2020**, *11*, 5934.
[193] S. Lee, R. Peng, C. Wu, M. Li, *Nat. Commun.* **2022**, *13*, 1485.
[194] F. Liao, Z. Zhou, B. J. Kim, J. Chen, J. Wang, T. Wan, Y. Zhou, A. T. Hoang, C. Wang, J. Kang, J. Ahn, Y. Chai, *Nat. Electron.* **2022**, *5*, 84.
[195] P. Li, M. Zhang, Q. Zhou, Q. Zhang, D. Xie, G. Li, Z. Liu, Z. Wang, E. Guo, M. He, C. Wang, L. Gu, G. Yang, K. Jin, C. Ge, *Nat. Commun.* **2024**, *15*, 3257.
[196] D. Hao, J. Zhang, S. Dai, J. Zhang, J. Huang, *ACS Appl. Mater. Interfaces.* **2020**, *12*, 39487.
[197] Y. Sun, L. Qian, D. Xie, Y. Lin, M. Sun, W. Li, L. Ding, T. Ren, T. Palacios, *Adv. Funct. Mater.* **2019**, *29*, 1902538.
[198] J. Y. Chen, Y. C. Chiu, Y. T. Li, C. C. Chueh, W. C. Chen, *Adv. Mater.* **2017**, *29*, 1702217.
[199] Z. Chen, Y. Zhang, Y. Yu, M. Cao, Y. Che, L. Jin, Y. Li, Q. Li, T. Li, H. Dai, J. Yang, J. Yao, *Appl. Phys. Lett.* **2019**, *114*, 181103.
[200] L. Qian, Y. Sun, M. Wu, C. Li, D. Xie, L. Ding, G. Shi, *Nanoscale.* **2018**, *10*, 6837.
[201] H. Shao, Y. Li, J. Zhuang, Y. Ji, X. He, R. Wang, L. Wang, J. Fu, W. Li, M. Yi, L. Xie, W. Huang, H. Ling, *Adv. Funct. Mater.* **2024**, *34*, 2316381.
[202] B. Yang, Y. Lu, D. Jiang, Z. Li, Y. Zeng, S. Zhang, Y. Ye, Z. Liu, Q. Ou, Y. Wang, S. Dai, Y. Yi, J. Huang, *Adv. Mater.* **2020**, *32*, 2001227.
[203] B. H. Jeong, J. Park, D. Kim, J. Lee, I. H. Jung, H. J. Park, *Adv. Opt. Mater.* **2024**, *12*, 2301652.
[204] X. Wu, S. Wang, W. Huang, Y. Dong, Z. Wang, W. Huang, *Nat. Commun.* **2023**, *14*, 468.
[205] T. Jiang, Y. Wang, Y. Zheng, L. Wang, X. He, L. Li, Y. Deng, H. Dong, H. Tian, Y. Geng, L. Xie, Y. Lei, H. Ling, D. Ji, W. Hu, *Nat. Commun.* **2023**, *14*, 2281.
[206] S. Dai, X. Wu, D. Liu, Y. Chu, K. Wang, B. Yang, J. Huang, *ACS Appl. Mater. Interfaces.* **2018**, *10*, 21472.
[207] L. Fang, S. Dai, Y. Zhao, D. Liu, J. Huang, *Adv. Electron. Mater.* **2020**, *6*, 1901217.
[208] Y. Wang, J. Yang, W. Ye, D. She, J. Chen, Z. Lv, V. A. L. Roy, H. Li, K. Zhou, Q. Yang, Y. Zhou, S. T. Han, *Adv. Electron. Mater.* **2020**, *6*, 1900765.

 © 2024 The Author(s). Advanced Electronic Materials published by Wiley-VCH GmbH

2199160x, 2025, 3, Downloaded from https://advanced.onlinelibrary.wiley.com/doi/10.1002/aelm.202400482 by HONG KONG POLYTECHNIC UNIVERSITY HU NG HOM, Wiley Online Library on [24/02/2026]. See the Terms and Conditions (https://onlinelibrary.wiley.com/terms-and-conditions) on Wiley Online Library for rules of use; OA articles are governed by the applicable Creative Commons License

[209] J. Zhang, P. Guo, Z. Guo, L. Li, T. Sun, D. Liu, L. Tian, G. Zu, L. Xiong, J. Zhang, J. Huang, *Adv. Funct. Mater.* **2023**, *33*, 2302885.
[210] J. H. Jeong, J. H. Ma, M. H. Park, H. J. Ha, S. J. Kang, J. M. Yun, Y. B. Kim, E. Kim, S. J. Kang, *Adv. Funct. Mater.* **2024**, 2402222.
[211] Z. Ni, Y. Wang, L. Liu, S. Zhao, Y. Xu, X. Pi, D. Yang, *Proc. 2018 IEEE Int. Electron Devices Meeting (IEDM)*, IEEE, San Francisco, CA, USA **2018**, 3851.
[212] Y. Zhai, Y. Zhou, X. Yang, F. Wang, W. Ye, X. Zhu, D. She, W. D. Lu, S. Han, *Nano Energy.* **2020**, *67*, 104262.
[213] H. Duan, K. Javaid, L. Liang, L. Huang, J. Yu, H. Zhang, J. Gao, F. Zhuge, T. Chang, H. Cao, *Phys. Status Solidi RRL.* **2020**, *14*, 1900630.
[214] Q. Wang, Y. Wen, K. Cai, R. Cheng, L. Yin, Y. Zhang, J. Li, Z. Wang, F. Wang, F. Wang, T. A. Shifa, C. Jiang, H. Yang, J. He, *Sci. Adv.* **2018**, *4*, eaap7916.
[215] B. Mu, L. Guo, J. Liao, P. Xie, G. Ding, Z. Lv, Y. Zhou, S. T. Han, Y. Yan, *Small.* **2021**, *17*, 2103837.
[216] T. Ahmed, M. Tahir, M. X. Low, Y. Ren, S. A. Tawfik, E. Mayes, S. Kuriakose, S. Nawaz, M. Spencer, H. Chen, M. Bhaskaran, S. Sriram, S. Walia, *Adv. Mater.* **2021**, *33*, 2004207.
[217] Y. Hou, Y. Li, Z. Zhang, J. Li, D. Qi, X. Chen, J. Wang, B. Yao, M. Yu, T. Lu, J. Zhang, *ACS Nano.* **2021**, *15*, 1497.
[218] J. Liang, X. Yu, J. Qiu, M. Wang, C. Cheng, B. Huang, H. Zhang, R. Chen, W. Pei, H. Chen, *ACS Appl. Mater. Interfaces* **2023**, *15*, 9584.
[219] Z. Wen, S. Wang, F. Yi, D. Zheng, C. Yan, Z. Sun, *ACS Appl. Mater. Interfaces.* **2023**, *15*, 55916.
[220] S. Hong, S. H. Choi, J. Park, H. Yoo, J. Y. Oh, E. Hwang, D. H. Yoon, S. Kim, *ACS Nano.* **2020**, *14*, 9796.
[221] Y. Zhang, B. Wang, Z. Han, X. Shi, N. Zhang, T. Miao, D. Lin, Z. Jiang, M. Liu, H. Guo, J. Zhang, H. Hu, L. Wang, *ACS Photonics.* **2023**, *10*, 1575.
[222] D. Li, H. Ren, Y. Chen, Y. Tang, K. Liang, Y. Wang, F. Li, G. Liu, L. Meng, B. Zhu, *Adv. Funct. Mater.* **2023**, *33*, 2303198.
[223] R. Wu, X. Liu, Y. Yuan, Z. Wang, Y. Jing, J. Sun, *Adv. Funct. Mater.* **2023**, *33*, 2305677.
[224] S. M. Kwon, J. Y. Kwak, S. Song, J. Kim, C. Jo, S. S. Cho, S. J. Nam, J. Kim, G. S. Park, Y. H. Kim, S. K. Park, *Adv. Mater.* **2021**, *33*, 2105017.
[225] Y. Tan, H. Hao, Y. Chen, Y. Kang, T. Xu, C. Li, X. Xie, T. Jiang, *Adv. Mater.* **2022**, *34*, 2206816.
[226] Y. C. Mi, C. H. Yang, L. C. Shih, J. S. Chen, *Adv. Opt. Mater.* **2023**, *11*, 2300089.
[227] Z. Gao, R. Jiang, M. Deng, C. Zhao, Z. Hong, L. Shang, Y. Li, L. Zhu, J. Zhang, J. Zhang, Z. Hu, *Adv. Mater.* **2024**, *36*, 2401585.
[228] L. Gu, Y. Li, D. Xie, J. Jiang, *IEEE Trans. Electron Devices.* **2022**, *69*, 4382.
[229] Y. Chen, M. Zhang, D. Li, Y. Tang, H. Ren, J. Li, K. Liang, Y. Wang, L. Wen, W. Li, W. Kong, S. Liu, H. Wang, D. Wang, B. Zhu, *ACS Nano.* **2023**, *17*, 12499.
[230] H. Lai, Y. Zhou, H. Zhou, N. Zhang, X. Ding, P. Liu, X. Wang, W. Xie, *Adv. Mater.* **2022**, *34*, 2110278.
[231] S. Rehman, M. A. Khan, H. Kim, H. Patil, J. Aziz, K. D. Kadam, M. A. Rehman, M. Rabeel, A. Hao, K. Khan, S. Kim, J. Eom, D. K. Kim, M. F. Khan, *Adv. Sci.* **2023**, *10*, 2205383.
[232] D. A. Nguyen, S. Cho, S. Park, D. Y. Park, H. C. Suh, M. S. Jeong, T. P. Anh Bach, H. Kim, H. Im, *Nano Energy.* **2023**, *113*, 108552.
[233] X. Pang, Y. Wang, Y. Zhu, Z. Zhang, D. Xiang, X. Ge, H. Wu, Y. Jiang, Z. Liu, X. Liu, C. Liu, W. Hu, P. Zhou, *Nat. Commun.* **2024**, *15*, 1613.
[234] L. Pi, P. Wang, S. Liang, P. Luo, H. Wang, D. Li, Z. Li, P. Chen, X. Zhou, F. Miao, T. Zhai, *Nat. Electron.* **2022**, *5*, 248.
[235] M. Tsai, C. Huang, C. Lin, M. Lee, F. Yang, M. Li, Y. Chang, K. Watanabe, T. Taniguchi, C. Ho, W. Wu, M. Yamamoto, J. Wu, P. Chiu, Y. Lin, *Nat. Electron.* **2023**, *6*, 755.
[236] Y. Yang, C. Pan, Y. Li, X. Yangdong, P. Wang, Z. Li, S. Wang, W. Yu, G. Liu, B. Cheng, Z. Di, S. Liang, F. Miao, *Nat. Electron.* **2024**, *7*, 225.
[237] Z. Zhang, S. Wang, C. Liu, R. Xie, W. Hu, P. Zhou, *Nat. Nanotechnol.* **2022**, *17*, 27.
[238] C. Wang, S. Liang, S. Wang, P. Wang, Z. Li, Z. Wang, A. Gao, C. Pan, C. Liu, J. Liu, H. Yang, X. Liu, W. Song, C. Wang, B. Cheng, X. Wang, K. Chen, Z. Wang, K. Watanabe, T. Taniguchi, J. J. Yang, F. Miao, *Sci. Adv.* **2020**, *6*, eaba6173.
[239] G. X. Zhang, Z. C. Zhang, X. D. Chen, L. Kang, Y. Li, F. D. Wang, L. Shi, K. Shi, Z. B. Liu, J. G. Tian, T. B. Lu, J. Zhang, *Sci. Adv.* **2023**, *9*, eadi5104.
[240] H. Jang, H. Hinton, W. Jung, M. Lee, C. Kim, M. Park, S. Lee, S. Park, D. Ham, *Nat. Electron.* **2022**, *5*, 519.
[241] X. Zhu, C. Gao, Y. Ren, X. Zhang, E. Li, C. Wang, F. Yang, J. Wu, W. Hu, H. Chen, *Adv. Mater.* **2023**, *35*, 2301468.
[242] R. Yang, Y. Wang, S. Li, D. Hu, Q. Chen, F. Zhuge, Z. Ye, X. Pi, J. Lu, *Adv. Funct. Mater.* **2024**, *34*, 2312444.
[243] R. Ji, G. Feng, C. Jiang, B. Tian, C. Luo, H. Lin, X. Tang, H. Peng, C. G. Duan, *Adv. Electron. Mater.* **2022**, *8*, 2101402.
[244] S. Sun, T. Zhang, S. Jin, X. Pan, J. Lu, Z. Ye, B. Lu, *Adv. Funct. Mater.* **2024**, 2401403.
[245] C. H. Zhu, X. Gao, H. T. Huang, L. X. Li, J. L. Xu, Y. N. Zhong, W. Tang, X. J. Guo, S. D. Wang, *Adv. Mater. Technol.* **2023**, *8*, 2300187.
[246] S. Ge, F. Huang, J. He, Z. Xu, Z. Sun, X. Han, C. Wang, L. B. Huang, C. Pan, *Adv. Opt. Mater.* **2022**, *10*, 2200409.
[247] T. Dixit, A. Tripathi, K. L. Ganapathi, M. S. R. Rao, V. Singh, *IEEE Photonics Technol. Lett.* **2020**, *32*, 329.
[248] I. Nikolaev, A. Kazakov, K. Drozdov, M. Bannikov, K. Spirin, R. Menshchikov, S. Dvoretsky, N. Mikhailov, D. Khokhlov, A. Ikonnikov, *J. Appl. Phys.* **2022**, *132*, 234301.
[249] H. Li, X. Jiang, W. Ye, H. Zhang, L. Zhou, F. Zhang, D. She, Y. Zhou, S. Han, *Nano Energy.* **2019**, *65*, 104000.
[250] B. Cui, Z. Fan, W. Li, Y. Chen, S. Dong, Z. Tan, S. Cheng, B. Tian, R. Tao, G. Tian, D. Chen, Z. Hou, M. Qin, M. Zeng, X. Lu, G. Zhou, X. Gao, J. M. Liu, *Nat. Commun.* **2022**, *13*, 1707.
[251] Y. Hu, M. Dai, W. Feng, X. Zhang, F. Gao, S. Zhang, B. Tan, J. Zhang, Y. Shuai, Y. Fu, P. Hu, *Adv. Mater.* **2021**, *33*, 2104960.
[252] S. Wang, H. Chen, T. Liu, Y. Wei, G. Yao, Q. Lin, X. Han, C. Zhang, H. Huang, *Angew. Chem., Int. Ed.* **2023**, *62*, 202213733.
[253] H. Tan, Z. Ni, W. Peng, S. Du, X. Liu, S. Zhao, W. Li, Z. Ye, M. Xu, Y. Xu, X. Pi, D. Yang, *Nano Energy.* **2018**, *52*, 422.
[254] H. S. Zhang, X. M. Dong, Z. C. Zhang, Z. P. Zhang, C. Y. Ban, Z. Zhou, C. Song, S. Q. Yan, Q. Xin, J. Q. Liu, Y. X. Li, W. Huang, *Nat. Commun.* **2022**, *13*, 4996.
[255] C. M. Yang, T. C. Chen, D. Verma, L. J. Li, B. Liu, W. H. Chang, C. S. Lai, *Adv. Funct. Mater.* **2020**, *30*, 2001598.
[256] B. Dang, K. Liu, X. Wu, Z. Yang, L. Xu, Y. Yang, R. Huang, *Adv. Mater.* **2023**, *35*, 2204844.
[257] K. He, Y. Liu, J. Yu, X. Guo, M. Wang, L. Zhang, C. Wan, T. Wang, C. Zhou, X. Chen, *ACS Nano.* **2022**, *16*, 9691.
[258] C. Liao, W. Wang, Y. Sun, Y. Wang, S. Liu, P. Tong, Q. Li, *Adv. Intell. Syst.* **2023**, *5*, 2200298.
[259] S. Chen, Z. Lou, D. Chen, G. Shen, *Adv. Mater.* **2018**, *30*, 1705400.
[260] L. Wu, Z. Wang, B. Wang, Q. Chen, L. Bao, Z. Yu, Y. Yang, Y. Ling, Y. Qin, K. Tang, Y. Cai, R. Huang, *Nanoscale.* **2021**, *13*, 3483.
[261] Z. Zhang, X. Zhao, X. Zhang, X. Hou, X. Ma, S. Tang, Y. Zhang, G. Xu, Q. Liu, S. Long, *Nat. Commun.* **2022**, *13*, 6590.
[262] T. Wang, J. Meng, X. Zhou, Y. Liu, Z. He, Q. Han, Q. Li, J. Yu, Z. Li, Y. Liu, H. Zhu, Q. Sun, D. W. Zhang, P. Chen, H. Peng, L. Chen, *Nat. Commun.* **2022**, *13*, 7432.
[263] Y. Wang, Y. Gong, S. Huang, X. Xing, Z. Lv, J. Wang, J. Yang, G. Zhang, Y. Zhou, S. Han, *Nat. Commun.* **2021**, *12*, 5979.
[264] D. Dev, A. Krishnaprasad, M. S. Shawkat, Z. He, S. Das, D. Fan, H. Chung, Y. Jung, T. Roy, *IEEE Electron Device Lett.* **2020**, *41*, 936.
[265] A. Sengupta, S. H. Choday, Y. Kim, K. Roy, *Appl. Phys. Lett.* **2015**, *106*, 143701.

© 2024 The Author(s). Advanced Electronic Materials published by Wiley-VCH GmbH

2199160x, 2025, 3, Downloaded from https://advanced.onlinelibrary.wiley.com/doi/10.1002/aelm.202400482 by HONG KONG POLYTECHNIC UNIVERSITY HU NG HOM, Wiley Online Library on [24/02/2026]. See the Terms and Conditions (https://onlinelibrary.wiley.com/terms-and-conditions) on Wiley Online Library for rules of use; OA articles are governed by the applicable Creative Commons License

[266] H. Mulaosmanovic, E. Chicca, M. Bertele, T. Mikolajick, S. Slesazeck, *Nanoscale.* **2018**, *10*, 21755.
[267] V. Benfenati, S. Toffanin, S. Bonetti, G. Turatti, A. Pistone, M. Chiappalone, A. Sagnella, A. Stefani, G. Generali, G. Ruani, D. Saguatti, R. Zamboni, M. Muccini, *Nat. Mater.* **2013**, *12*, 672.
[268] C. Qian, L. Kong, J. Yang, Y. Gao, J. Sun, *Appl. Phys. Lett.* **2017**, *110*, 83302.
[269] H. Li, J. Hu, Y. Zhang, A. Chen, J. Zhou, Y. Zhao, Y. Xu, B. Yu, *Adv. Funct. Mater.* **2024**, *34*, 2314456.
[270] D. Lee, M. Park, Y. Baek, B. Bae, J. Heo, K. Lee, *Nat. Commun.* **2022**, *13*, 5223.
[271] F. Li, D. Li, C. Wang, G. Liu, R. Wang, H. Ren, Y. Tang, Y. Wang, Y. Chen, K. Liang, Q. Huang, M. Sawan, M. Qiu, H. Wang, B. Zhu, *Nat. Commun.* **2024**, *15*, 3689.
[272] J. Chen, Z. Zhou, B. J. Kim, Y. Zhou, Z. Wang, T. Wan, J. Yan, J. Kang, J. H. Ahn, Y. Chai, *Nat. Nanotechnol.* **2023**, *18*, 882.
[273] Y. Wang, Y. Gong, S. Huang, X. Xing, Z. Lv, J. Wang, J. Q. Yang, G. Zhang, Y. Zhou, S. T. Han, *Nat. Commun.* **2021**, *12*, 5979.
[274] J. Robertson, Y. Zhang, M. Hejda, J. Bueno, S. Xiang, A. Hurtado, *Opt. Express.* **2020**, *28*, 37526.
[275] J. Robertson, M. Hejda, J. Bueno, A. Hurtado, *Sci. Rep.* **2020**, *10*, 6098.
[276] J. Robertson, E. Wade, Y. Kopp, J. Bueno, A. Hurtado, *IEEE J. Sel. Top. Quantum Electron.* **2020**, *26*, 7700715.
[277] J. Robertson, E. Wade, A. Hurtado, *Proc. 2019 IEEE Photonics Conference (IPC)*, IEEE, San Antonio, TX, USA **2019**.
[278] A. Hurtado, J. Javaloyes, *Appl. Phys. Lett.* **2015**, *107*, 241103.
[279] M. A. Nahmias, B. J. Shastri, A. N. Tait, P. R. Prucnal, *IEEE J. Sel. Top. Quantum Electron.* **2013**, *19*, 1800212.
[280] V. N. Chizhevsky, V. A. Kulchitsky, S. Y. Kilin, *Appl. Phys. Lett.* **2021**, *119*, 041107.
[281] C. Mesaritakis, A. Kapsalis, A. Bogris, D. Syvridis, *Sci. Rep.* **2016**, *6*, 39317.

Lingxiang Hu received his Ph.D. degree in Materials Science from the University of Chinese Academy of Sciences in 2021. He then became a postdoctoral fellow in the Ningbo Institute of Materials Technology and Engineering, Chinese Academy of Sciences. His current research interests focus on optoelectronic memristor and brain-inspired computing.

Xia Zhuge received her Ph.D. degree in Information Engineering from the Hiroshima University, Hiroshima, Japan, in 2011. Since 2011, she has been an Associate Professor in the School of Electronic and Information Engineering, Ningbo University of Technology. Her current research interests focus on memristive artificial neural networks.

Xiaoyong Xue (Member, IEEE) received his Ph.D. degree in microelectronics from the Fudan University, China, in 2011. He joined the Department of Microelectronics at Fudan University as a postdoctoral research fellow. He is now an Associate Professor at the Fudan University. His research interests include high-performance memory/storage, in-memory computing circuits, and systems.

© 2024 The Author(s). Advanced Electronic Materials published by Wiley-VCH GmbH

2199160x, 2025, 3, Downloaded from https://advanced.onlinelibrary.wiley.com/doi/10.1002/aelm.202400482 by HONG KONG POLYTECHNIC UNIVERSITY HU NG HOM, Wiley Online Library on [24/02/2026]. See the Terms and Conditions (https://onlinelibrary.wiley.com/terms-and-conditions) on Wiley Online Library for rules of use; OA articles are governed by the applicable Creative Commons License

ADVANCED ELECTRONIC MATERIALS Open Access
www.advelectronicmat.de

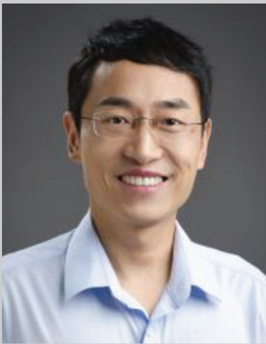

Fei Zhuge received his Ph.D. degree in Materials Science from the Zhejiang University, China, in 2005. He then became a JSPS postdoctoral fellow in the Hiroshima University, Hiroshima, Japan. He joined the Ningbo Institute of Materials Technology and Engineering (NIMTE), Chinese Academy of Sciences (CAS) in 2008. Since 2014, he has been a professor at NIMTE. Since 2018, he has been a Guest Professor at the Center for Excellence in Brain Science and Intelligence Technology, CAS. His current research interests include low-dimensional semiconductor materials and devices, memristive materials and devices, and brain-inspired artificial intelligence.

 © 2024 The Author(s). Advanced Electronic Materials published by Wiley-VCH GmbH

2199160x, 2025, 3, Downloaded from https://advanced.onlinelibrary.wiley.com/doi/10.1002/aelm.202400482 by HONG KONG POLYTECHNIC UNIVERSITY HU NG HOM, Wiley Online Library on [24/02/2026]. See the Terms and Conditions (https://onlinelibrary.wiley.com/terms-and-conditions) on Wiley Online Library for rules of use; OA articles are governed by the applicable Creative Commons License